MATERIAL CHARACTERIZATION FOR COMPOSITE MATERIALS IN LOAD BEARING WAVE GUIDES

THESIS

Gabriel Almodovar, Captain, USAF

AFIT/GAE/ENY/12-M01

DEPARTMENT OF THE AIR FORCE
AIR UNIVERSITY

AIR FORCE INSTITUTE OF TECHNOLOGY

Wright-Patterson Air Force Base, Ohio

AFIT/GAE/ENY/12-M22

MATERIAL CHARACTERIZATION FOR COMPOSITE MATERIALS IN LOAD BEARING WAVE GUIDES

THESIS

Presented to the Faculty

Department of Aeronautics and Astronautics

Graduate School of Engineering and Management

Air Force Institute of Technology

Air University

Air Education and Training Command

In Partial Fulfillment of the Requirements for the

Degree of Master of Science in Aeronautical Engineering

Gabriel Almodovar, BS

Captain, USAF

March 2012

AFIT/GAE/ENY/12-M01

MATERIAL CHARACTERIZATION FOR COMPOSITE MATERIALS IN LOAD BEARING WAVE GUIDES

Gabriel Almodovar, BS
Captain, USAF

Approved:

_____	_____
Dr Anthony Palazotto (Chairman)	Date
_____	_____
Dr Khalid Lafdi (Member)	Date
_____	_____
Maj Milo Hyde USAF (Member)	Date

Abstract

This study will establish a methodology to examine samples of composite material for application in a load bearing waveguide. The composite material will operate in a specific frequency range for applications in small RPAs. A graphite epoxy stiffening component will be primarily considered. Different nickel, graphene, and carbon nanotube (CNT) coatings and films will be applied to the graphite epoxy. Tests will determine the material's radio frequency (RF) performance for application as an antenna/waveguide component. The study will use scattering (S) parameters determined from a network analyzer to collect these data. The S parameters will then be used to resolve the composites permittivity and reflectivity and allow an estimation of a full scale waveguides performance made from pretested composite material.

Acknowledgements

Throughout this thesis effort, numerous people have given me overwhelming help and support. My faculty advisor, Dr Anthony Palazotto, helped me through each obstacle I encountered. A special thanks goes out to Maj Milo Hyde. Without his patience and knowledge, I would not have been able to complete this work. Dr Khalid Lafdi provided technical expertise and needed advice. The AFIT laboratory staff always provided me with the tools, experience, and expertise needed. My fiancée, family, and friends: without them, this would not be possible. Through the rigorous curriculum, they ensured I stayed grounded and focused on what truly matters in life. Whether it was weekend trips, Sunday fundays, loving gestures, support, or just their understanding, I sincerely appreciate everyone's help and appreciate all of the time and effort spent on this project. Finally, I would like to thank all the FOB and deployed service members both home and abroad…get home safe.

Gabe Almodovar

Table of Contents

Page

List of Figures

Page

List of Tables

Page

List of Symbols

Symbol	
ε_o	Permittivity of free space
D	Electric flux density
t	Sample thickness
A	Antenna area
R	Radar range
P_s	Power transmitted
λ	Wavelength
P_e	Received power
o	Target radar cross-section
σ	Conductivity
∇	Del operator
ρ_v	Electric charge density per unit volume
E	Electric field intensity
B	Magnetic field density
H	Magnetic field intensity
J	Current density per unit area
μ	Permeability
ε	Permittivity
eV	Electronvolts
$[b_i]$	Network output signal matrix
$[a_i]$	Network input signal matrix
a	Widest dimension of waveguide opening
b	Smallest dimension of waveguide opening
[S]	Scatter parameter matrix
$\boldsymbol{S_{ij}}$	Scatter parameter received at port i and sent from port j (complex number)
Γ	Reflection coefficient
K	Specific group of terms used to simplify
Λ	Specific group of terms used to simplify

T	Transmission coefficient
μ_r	Relative permeability
ε_r	Relative permittivity
λ_c	Cutoff wavelength
λ_o	Free-space wavelength
c	Speed of light
f_c	Cutoff frequency
μ_0	Permeability of free-space
α_t	Total attenuation constant
α_d	Dielectric attenuation
α_c	Conduction (ohmic) losses
η	Intrinsic impedance
R_s	Sheet resistivity
f	Frequency
N	Sample size
s	Standard deviation
$\bar{X}$	Sample mean
x_i	Specific measurement from a sample set
z	Arbitrary representation of any measurement
$t_{\alpha/2}$	Area of the tail end of a T distribution curve
Z_0	System impedance
δ_s	Skin depth

List of Abbreviations

Abbreviation

AFIT	Air Force Institute of Technology
AFRL	Air Force Research Laboratory
DoD	Department of Defense
CLAS	Conformal Load-bearing Antenna Structure
EM	Electromagnetic
ISR	Intelligence, Surveillance, and Reconnaissance
SWASS	Slotted Waveguide Antenna Stiffened Structure
RPA	Remotely Piloted Aircraft
CFRP	Carbon Fiber-Reinforced Plastic
eV	electronvolts
SAR	Synthetic Aperture Radar
DARPA	Defense Advanced Research Projects Agency
ISR	Intelligence, Surveillance, and Reconnaissance
ISIS	Integrated Sensor Is Structure
MUSTRAP	Multifunctional Structural Aperture
MWCNT	Multi-walled Carbon Nanotube
SWCNT	Single-walled Carbon Nanotube
NASA	National Aeronautics and Space Administration
CNT	Carbon Nanotube
GNR	Graphene Nanoribbons
TRM	Transmission Reflection Method
NRW	Nicolson-Ross-Weir
LO	Low Observables
TRL	Thru-Reflect-Line
RF	Radio Frequency
dB	Decibels
Np	Nepers
GHz	Gigahertz

MATERIAL CHARACTERIZATION FOR COMPOSITE MATERIALS IN LOAD BEARING WAVE GUIDES

I. Introduction

The Department of Defense (DoD) and United States intelligence agencies have increasingly depended on the electromagnetic spectrum to conduct combat and intelligence operations. Antenna arrays are important tool for communications and Intelligence, Surveillance, and Reconnaissance (ISR). These assets are in high demand because the military and analysts depend on the images, video, voice, and radar data these assets provide. These antenna components add significant weight and cost in procurement and operation to these assets. Thus, the aerospace industry has looked at using composite materials to form multifunctional components, i.e., components capable of meeting multiple requirements, to cut down on costs. One such concept is a conformal load-bearing antenna structure (CLAS). The purpose of a CLAS is to perform the function of both a support structure, capable of taking loads, and an antenna, capable of transmitting/receiving electromagnetic (EM) waves. One such project is under way at the Air Force Research Lab (AFRL) in which a hat stiffener support on aircraft skin panels is combined with a slotted waveguide. This program is called the Slotted Waveguide Antenna Stiffened Structure (SWASS). This research will look into the feasibility and performance of carbon based materials and composites in waveguide applications with the goal of finding composites capable of adequately performing the waveguide function. The purpose is to establish procedures for developing methods to evaluate alternative materials for use as lightweight load carrying composite waveguides.

1.1 Motivation for research

The increased need for persistent ISR assets and the future fiscal constraints requires aerospace systems to operate more functions more efficiently. In addition, there has been a dramatic increase in remotely piloted vehicles (RPAs), and are being designed to be lighter and more capable. The SWASS can provide aerospace assets with the ability to accomplish their mission more efficiently. Many aerospace systems have been designed in such a way that one component achieves one function. This is because of the difficulty in designing multifunctional components that often times have competing requirements.

Today's military systems posses increasingly sophisticated radar systems. These radar systems and antenna are part of a system of systems. For many aircraft, antenna components must be integrated in the platform by adding an additional housing outside the desired aerodynamic shape of the aircraft. These additional components pose not only a weight penalty but can significantly add drag, both of which drive up the cost of maintaining and operating the aircraft. A SWASS system could reduce or eliminate the need of an additional housing for the radar antenna components. This will increase the overall system efficiency by requiring less weight and a smaller total area for the radar components. [18] The potential for weight savings, increased capability, and the resulting reduction in life cycle cost are primary reasons for pursuing such multi-functional designs.

Integrating antenna waveguides and skin structure could increase the overall radar's performance by increasing the antenna area. Equation (1) is the radar range equation. From this, we can determine that a two fold increase in the frontal area of the antenna, *A*, would improve the range, *R*, by 41% while doubling the transmitted power,P_s, only increases the range by 19%. [18]

$$R = \sqrt[4]{\frac{P_s \pi^2 A^2 o}{4\pi^3 P_e \lambda^2}} \quad (1)$$

On today's battlefield, combatant commanders demand the data ISR and radar assets provide. This demand has placed added stress on the low-density assets currently in the inventory. While these assets provide the needed info, future platforms will be required to provide more data and capabilities. With the current fiscal realities, future systems must be able to do more with less.

1.2 What is a Waveguide

A waveguide is a device used to transmit electromagnetic waves (or other types of waves) from one point to another. The waveguide acts as a conduit for this electromagnetic energy to travel through. A common type of waveguides is a hollow metal pipe used to carry electromagnetic waves, primarily radio frequency wave. [19] This is not the only type of waveguide. A fiber optic cable is a type of waveguide as is the coaxial cable connected to most television sets. Figure 1 shows a rectangular hollow waveguide with a 2.286 by 1.016 cm (.9" by .4") opening.

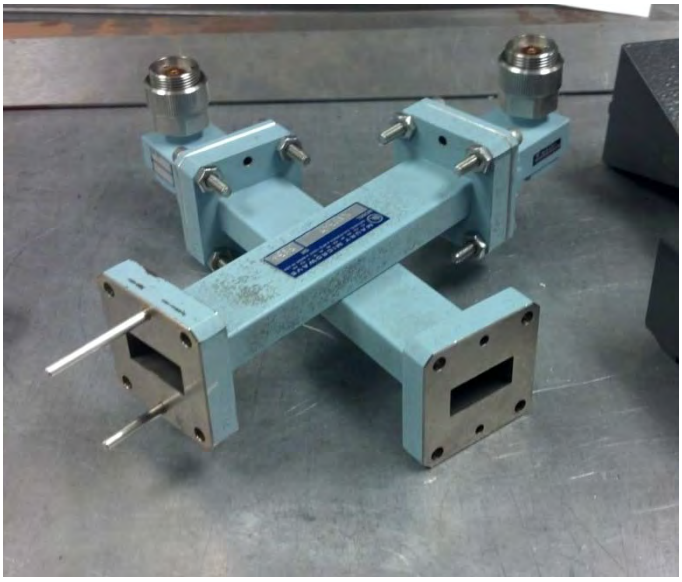

Figure 1: Hollow rectangular waveguides

The idea of the waveguide is for electromagnetic waves to enter one end and propagate to the other end of the waveguide with little or no loss in power. The waveguide works by reflecting the wave energy, which enters the guide, along the walls. There is a geometric relationship to what frequencies can enter and, therefore, propagate inside the waveguide based on the physical size of the waveguide opening. The frequency range is determined by its shape and dimension. Also, the inside lining material of the waveguide determines how efficiently it can transmit the electromagnetic energy. The inside material is responsible for reflecting the electromagnetic energy. Much like the way a bathroom mirror reflects light waves, the inside material ideally reflects the radio frequency (RF) waves. Depending on the inside material, it may resist and absorb much of the energy (create losses). This is very important in designing waveguides and waveguide structure and will be discussed in later chapters.

1.3 Composites

In early Egyptian times, straw and mud were combined and used to build housing. This early composite was unique because it combined two separate materials who themselves posses unique material properties. When put together, the “new” composite material was still made of two distinct materials, but their material properties combined to produce collective properties not achievable by either material alone. A composite is simply a "solid material which is composed of two or more substances having different physical characteristics and in which each substance retains its identity while contributing desirable properties to the whole." [20] Since a composite is made of two or more substances, it often times is difficult to characterize a composite's properties because by definition they are not homogeneous materials.

One class of composites is fiber-reinforced materials. Fiber reinforced composites consist of high strength fibers bonded to a matrix with distinct boundaries between them. The fibers are generally the load carrying members, while the surrounding matrix keeps them in the desired location and orientation. [8] This thesis will specifically examine carbon fiber-reinforced plastic (CFRP) composite materials.

There are several advantages to using CFRPs. The first and most well known is the high strength to weight ratio. Composites offer a greater strength to weight ratio than metals. For instance, Ti-6A1-4V titanium alloy has a tensile strength to weight ratio of $20.1 * 10^3$m compared to $101.9 * 10^3$m for a high strength carbon fiber epoxy, a fivefold increase. (Do note that these measurements are taken in the direction of the fiber.)

In fiber-reinforced composites, the mechanical properties strongly depend on the direction of the measurement because by definition composites are not isotropic materials. Because of the anisotropic nature of fiber-reinforced composites, the properties can be adapted according to design requirements. Metals on the other hand, are isotropic materials, and therefore, exhibit equal or nearly equal properties independent of the direction of measurement. [8] Impact strength, coefficient of thermal expansion, thermal conductivity, and others also depend on the direction at which they are measured.

Fiber composites have lower coefficient of thermal expansion than metals. This means a composite structure may exhibit a better dimensional stability over a wide temperature range. When using a composite with a metal, note that thermal stresses may result due to the differences in their thermal expansions. Fiber composites offer high internal damping, which leads to better "vibrational energy absorption within the material and results in reduced transmission of noise and vibrations to neighboring structures." [8] This is desirable in applications where noise and vibrations are issues. Another important advantage of composites is their non-corroding behavior. However, they can absorb moisture, which can create internal stresses. Composites are normally coated or painted to prevent moisture absorption.

Composites first started seeing use in military aircraft in 1969 as a boron fiber reinforced epoxy skin in F-14 horizontal stabilizers. [8] Since then, fiber-reinforced composites have seen a steady increase. The F-22 contains approximately 25% by weight of carbon fiber-reinforced composites, and the future Boeing 787 Dreamliner is expected to have about 50% by weight of composites. The steady rise of composite

components in aircraft is due to all the conducted research, the millions of flight hours parts have accumulated, and overall better understanding of them. This has led to an increase in confidence in a fiber-reinforced composite's structural integrity and durability. With an increased understanding of composites, you can begin to develop multifunctional components, such as a SWASS system. Such work aims to integrate the electromagnetic functionality into lightweight host structures and materials. [21]

Composites are made using a variety of techniques and forms. Some composites are made by layering unidirectional fiber sheets in which the desired mechanical properties are created by the number and orientation of the layers. Another method is to weave the fibers together. A woven fiber fabric is produced by intertwining fibers to form a specific pattern. Figure 2 shows four common weaves used in structural composites: (a) a unidirectional weave, (b) a 2-D plain weave, (c) a 2/2 twill weave, and (d) a four-harness satin weave. This research will utilize a 2-D weave.

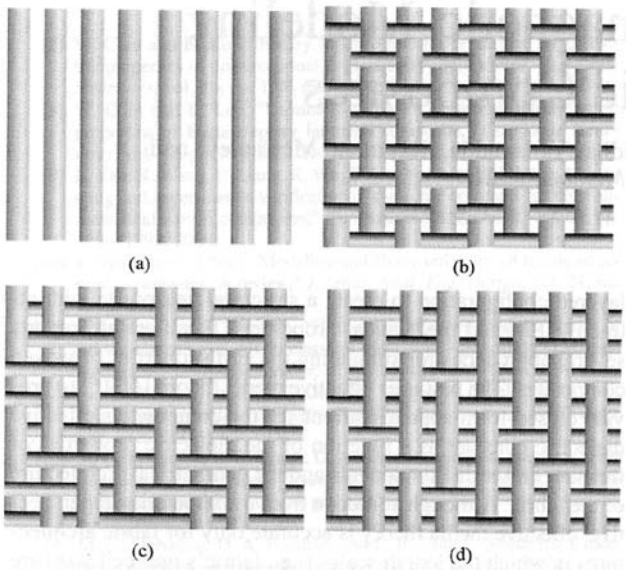

Figure 2: Common weave architectures

The choice of weave does effect the electromagnetic properties of the composite being designed. "The broadband EM properties are sensitive in the choice in fiber type, weave, bundle size, and bulk dielectric properties of the resin." [1] Research is being conducted to try to model not only a composite's mechanical properties but also its EM properties. "By tailoring the EM properties of structural composites (e.g., complex permittivity and permeability) it may be possible to integrate antennas, frequency selective surfaces, and other electromagnetic components directly into structural skin of future commercial and military vehicles and structures." [1] While this thesis does not analyze the effects and changes in EM properties from different weaves, fibers, and resins, it is important to note that these can greatly affect the EM properties of the composite. This research will however analyze the effects of different coating, films, and additives.

1.4 The SWASS Concept

The Slotted Waveguide Antenna Stiffened Structure program focuses on combining aircraft skin support structure with a slotted waveguide. A slotted waveguide differs from a regular hollow rectangular waveguide in that it is designed with slots on one side of the waveguide. As the EM energy travels down the waveguide, the slots are designed to allow the EM energy to escape or emit, in the case of this research RF energy. The SWASS concept aims to combine a slotted waveguide and a hat-stiffened panel. The hat-stiffened panel is designed to create a panel capable of handling the expected mechanical loads while minimizing weight and materials. Figure 3 shows a

typical slotted waveguide and hat-stiffened, panel and Figure 4 shows a conceptual picture of a SWASS component.

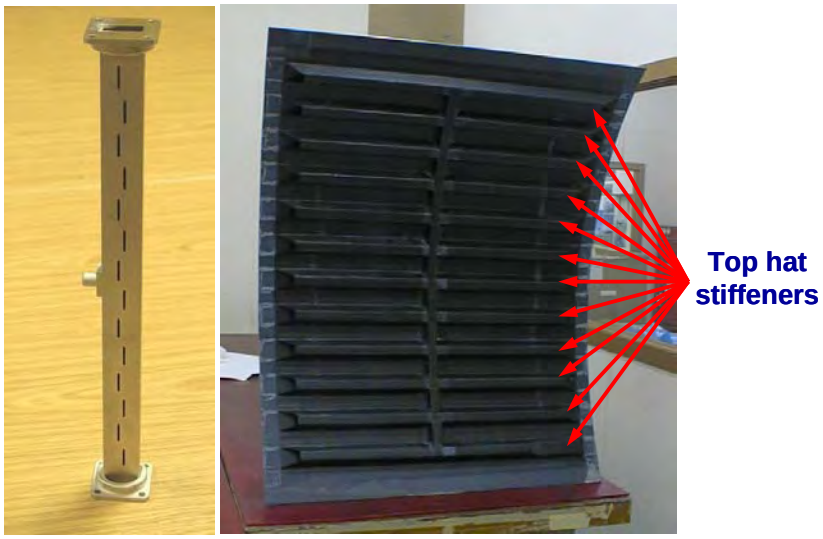

Figure 3: Slotted waveguide and hat stiffened panel

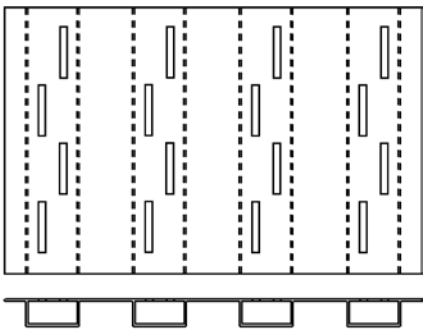

Figure 4: A conceptual SWASS component

1.5 CLAS Programs

There have been several CLAS programs that have researched and produced a system. One program used slotted waveguides as a structural antenna in a synthetic aperture radar (SAR) developed by Ericson and Dornier. [18] This system is designed for a satellite and to save weight was made from a carbon fiber reinforced plastic and metal

lining. The system was required to support its own weight when in the fully deployed configuration.

The Defense Advanced Research Program Agency (DARPA) has a program called the Integrated Sensor is Structure (ISIS). This program aims to "develop the technologies that enable extremely large lightweight phased-array radar antennas to be integrated into an airship platform." [21] This system is currently in design with an expected demonstration in 2013/14 timeframe.

The multifunction structural aperture (MUSTRAP) program structurally embedded an antenna in the vertical stabilizer of a NASA F-18, as shown in Figure 5.

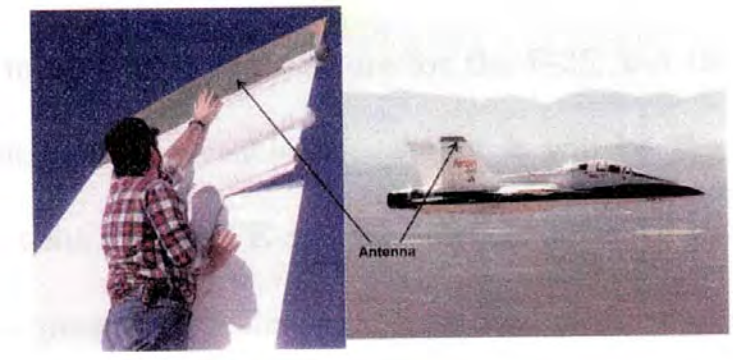

Figure 5: NASA F-18 with embedded MUSTRAP antenna

The program successfully flight tested the antenna and showed that it increased the radar performance by 15 to 25 dB because of the increase in the overall antenna size. [22]

There are significant benefits to load bearing sensors and antenna that can increase the efficiency of different platforms, and work continues to be done to develop these technologies.

1.6 Thesis Objective

The objective of this thesis is to establish a methodology to examine samples of composite material for application in a load bearing waveguide. The composite material will operate in the X band frequency range for applications in small RPAs. A graphite epoxy stiffening component will be considered with different carbon based coatings and films. Measurements will be performed to characterize the electrical properties of the composite. These measurements will collect scatter (S) parameter information using a network analyzer. The S parameters data will then be used to resolve the composites permittivity and reflectivity and allow an estimation of a full-scale waveguides performance made from pretested composite material.

II. Theory

The purpose of this chapter is to describe and understand some key principles that effect how a material reacts to applied electromagnetic (EM) energy. First, a brief introduction to electromagnetic theory and Maxwell's equations will be presented. This will outline the governing equations for EM waves themselves and serve as the basis for developing much of the theory to be presented. Then the chapter will cover the different material classifications, and the theory affecting a material's electrical properties. Next, the chapter will briefly describe the materials to be tested. This is followed by background information on the atomic structure and makeup of different carbon based materials and how it relates to its electrical properties. Lastly, a discussion of the theory pertaining to the test methods and algorithms used to characterize the material's reflectivity, conductivity, permittivity, and other electrical properties will be presented. The experiments required for determining a material's suitability in a waveguide application requires a basic understanding of material, electromagnetic, and physics principles.

2.1 Theory of Electromagnetic Wave Propagation

"The relations and variations of the electric and magnetic fields, charges, and currents associated with electromagnetic waves are governed by physical laws, which are known as Maxwell's equations." [6] Maxwell's equations describe, macroscopically, the connection between the electric field and electric charge, magnetic field and electric current, and the bilateral coupling between the electric and magnetic field quantities. [23]

These equations hold true for all materials, including free space, and at any (x,y,z) location. The general forms of Maxwell's equations are:

$$\nabla * D = \rho_v \quad (1)$$

$$\nabla \times E = -\frac{\partial B}{\partial t} \quad (2)$$

$$\nabla * B = 0 \quad (3)$$

$$\nabla \times H = J + \frac{\partial D}{\partial t} \quad (4)$$

where

E = electric field intensity

D = electric flux density

and $D = \varepsilon E$, where ε = electrical permittivity of the medium

H = magnetic field intensity

B = magnetic flux density

And $B = \mu H$, where μ =magnetic permeability of the medium

ρ_v = electric charge density per unit volume

J = current density per unit area

∇ = del operator

The electric flux density, *D*, is a measure of the strength of an electric field generated by a free electric charge. The Electric field intensity, *E*, is a measure for how strong an electric field is. The magnetic flux density, *B*, and magnetic field intensity, *H*, are the same as the electric flux density and electric field intensity but for the magnetic component of the EM wave. The current density per unit area, *J*, is just that. It is the

amount of current per unit area just as the electric charge density per unit volume, ρ_v, is the amount of electrical charge per unit volume. [23] The del operator,∇, can represent the gradient of a scalar field, the divergence of a vector field, or the curl of a vector field, depending on the application.

Maxwell's equations (1-4) explain the relationship between the electric and magnetic components of propagating waves. Figure 6 shows a graphical relationship between the electric and magnetic components described in Maxwell's equations.

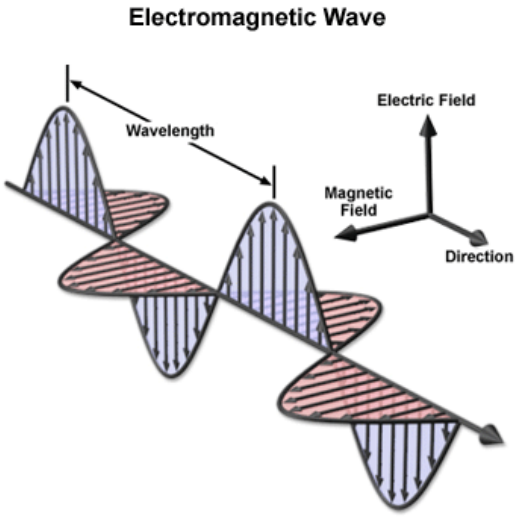

Figure 6: Electromagnetic wave in the electric and magnetic components

The electric and magnetic components impart energy onto any material but the effects of the EM energy depend on the type of material.

2.2 Material Classifications and Properties

Materials are classified according to their reaction to the electric and magnetic components described in Maxwell's equations, and the parameters that effect the propagation of EM waves through a material includes:

σ, material conductivity

ε, material permittivity

μ, material permeability

Conductivity is a measure of a materials ability to allow electric current to flow a material. Permittivity is a measure of a materials resistance to forming an electric field in the material (a low permittivity is desired for use in as the inside lining of a waveguide). Permeability is similar to permittivity. It measures a material's resistance to the magnetic field component of EM waves.

The materials can be categorized based on the magnitudes of their conductivities. The material classifications are conductors, semiconductors, and insulators (dielectrics). For example, a perfect electrical conductor is described as a material with no resistance to electric flows, $\sigma = \infty$. Conductors allow "free" or "lose" electrons to move throughout the material such that the net current is zero. A perfect insulator does not allow any electric flow through the material, $\sigma = 0$. At times in this thesis, semiconductors and insulators will be categorized together because conductors exhibit the desired electrical properties as opposed to semiconductors and insulators. A material's category depends on certain characteristics at the microscopic/atomic level.

Atoms "consist of a very small but massive nucleus that is surrounded by negatively charged electrons revolving about the nucleus and exert forces of attraction on

the positive charges of the nucleus." [6] These electrons exist in various shells or bands. Figure 7 shows a simple Bohr's model for a carbon atom in which the first band is referred to as the S band while the second band is referred to as the P band. Each material has a different arrangement and number of electrons that are located throughout the various bands not mentioned here, but each band can only have a certain maximum number of electrons.

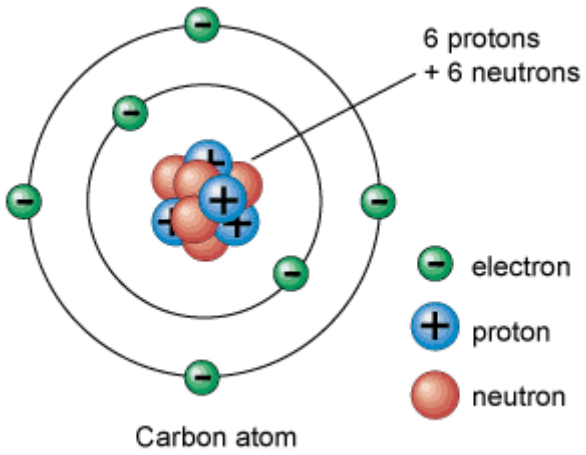

Figure 7: Bohr's model of a carbon atom

These bands represent different discrete energy levels. Bohr's model of an atom states that electrons can only exist in energy states that are determined by the radii of their orbital shells. The electron can change its energy band with the absorption or radiation of energy. This holds true in molecules, the minimum collection of atoms needed to form a specific material. In molecules, the process becomes a little more complex because of chemical bonds between the atoms but nonetheless still follow this idea.

The microscopic physical principals for the electrical properties of a material are "mainly determined by the electron energy bands of the material" [5] The energy gap between the valence and conduction band determines which classification a material falls into. The energy gap depends on the atomic structure and makeup of the atoms. The valence band is the atom's outer most band that contains electrons at zero degrees Kelvin. The conduction band is the discrete energy level at which an electron is "free" from the atomic forces of the nucleus/atom and free to flow throughout the lattice. It is at a higher energy level than the valence band. These two bands are separated by a gap referred to as the forbidden gap.

The primary difference between insulators, semiconductors, and conductors is the amount of energy required for an electron in the valence band to move to the conduction band. The larger the gap the more energy needed. Insulators have an energy gap greater than approximately 5 electronvolts (eV) compared to approximately 1eV for semiconductors and 0 eV for conductors. For instance, the valence and conductions bands overlap in conductors allowing electrons to become loose from their original atom with little or no energy. Figure 8 below shows a representation of the three types of materials.

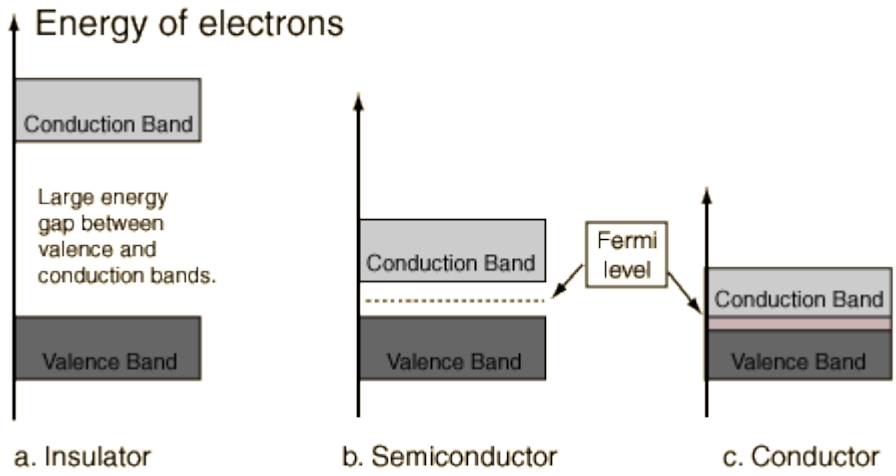

Figure 8: Energy band gap representation

Insulators, semiconductors, and conductors each behave differently when subjected to electromagnetic waves. Conductors usually have a conductivity between 10^4–10^8 ohms per meter while semiconducting materials have conductivity between 10^{-7} to 10^4 ohms per meter. For the purpose of this thesis and application, we will focus on the electric field components of Maxwell's equations, as opposed to the magnetic field components because permeability only affects ferrous materials, in which carbon is not. This means for nonferrous materials, the magnetic component of the EM waves have negligible affects in regards to this research. This allows the author to focus on insulators, conductors, polarization, and permittivity.

2.3 Electromagnetic Wave Propagation and Material Interaction

EM waves interact with a medium by transferring energy to the surface and into the medium. As discussed earlier, it does this in the form of electric and magnetic fields. These fields create currents, magnetic pulls, or magnetic pushes onto the material's

atomic structure and the internal protons and electrons. The additional energy from EM waves excites the electrons allowing them to potentially jump into higher energy bands or change their position relative to the nucleus. In addition, the EM waves create a time dependent alternating magnetic force on the material. The effects of the electric and magnetic forces depend on the type of material it is acting on.

When a material is subjected to an EM wave, the wave tries to create a current in the material. In a metals (conductor), there is very little resistivity to the generated current because metals have electrons that require little or no energy to become free electrons. The free electrons consolidate at the surface of the material and collectively oscillate as the EM wave propagates. This movement of electron creates a conduction current in the material. As described in Maxwell's equations, this current in turn generates a similar EM wave that propagates further down the material. In reality, some energy is lost in the form of heat in all materials, but ideally, the energy from the input EM wave is not wasted as heat. Instead, the energy is used to generate a current that (ideally) flows without resistance that then generates the same EM wave. Since most metals have very low resistivity, and the EM wave propagates along the surface.

In dielectric materials (insulators), the EM wave has a different effect because of how the material reacts to the applied energy/force. The nucleus and electrons require more energy to separate because the forbidden gap separating them is larger than in metals. Some of the electrons may become free from the EM wave energy but not all of them will. While the EM waves may not have enough energy to produce very many free electrons, the electric (and potentially magnetic) fields distort the atoms in the material. If we consider the nucleus of an atom to be fixed, the forces from the electric field will

alter the concentration of where the electrons will position themselves. This polarizes the atom as depicted in Figure 9.

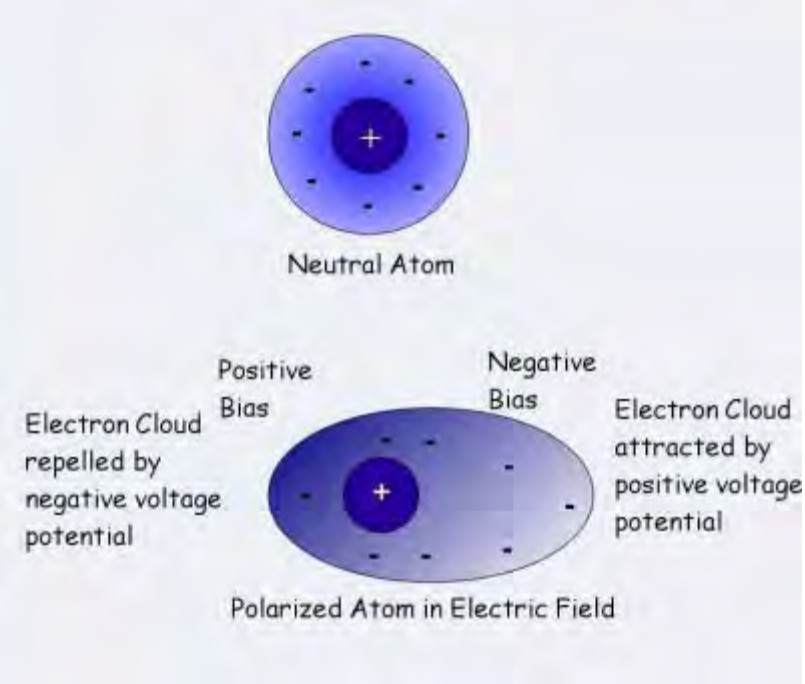

Figure 9: Atom in neutral state and polarized in an electric field

The distorted electrons can return to the original position once the applied EM field is removed, similar to a stretched spring. The energy to "stretch" the atom is stored and then released back in the form of energy once external forces are removed. This storage of energy is the principle behind capacitors, and permittivity quantifies this polarization. This polarization is also referred to as a displacement current. Another way to describe a good conductor is that its conduction current is significantly greater than the displacement current.

As discussed in previous sections, a materials reaction to the electric and magnetic field is quantified by the material parameters permittivity and permeability,

respectfully. While the atomic structure and forbidden gap play an important role in a material's response to EM waves, they do not dictate how a material will react under all circumstances. Permittivity, permeability, and conductance are also temperature and frequency dependent. The purpose of this study is to test carbon-based materials for their permittivity in the X-band frequency range at room temperature.

2.4 Materials under test

The focus of this research is to examine different coating, films, and materials to improve the electrical properties of composites. Previous research focused on mechanical properties of a slotted waveguide structure made of a composite. The composite was a resin reinforced plain-woven carbon fiber fabric made from Grafil 34-700 fibers and RS-36 epoxy resin. While the material performed adequately from a structural standpoint, it left much to be desired in terms of its electrical properties.
In this research, Grafil 34-700 fibers will be the fiber material. Due to logistical issues, the composites will use EPON 862 epoxy instead of the RS-36.

Grafil 34-700 is a carbon fiber with a tensile strength of 2572 MPa and a modulus of 137 GPa. The EPON 862epoxy resin is a low viscosity liquid epoxy resin. [27] All the materials will be made of a Grafil 34-700 2-D plain weave infused with the EPON 862 epoxy resin cured in an auto clave. The autoclave is a pressure vessel that subjects the composite to high pressure and temperature. This allows the resin and fiber fuse together. This process produces more consistent and better composites by reducing the voids within the resin and fiber.

The autoclave cured all the composites at .55 MPa (80 psi) and 121 degrees Celsius (250 Fahrenheit) for two hours followed by four hours at .55 MPa and 177 degrees Celsius (350 Fahrenheit) to complete the process. From this process, five different composites are manufactured: baseline composite, carbon nanotubes (CNTs) composite, nickel (Ni) coated CNTs composite, P100 fiber composite, and pyrolitic graphite composites. These are described in further detail in following sections.

.

2.4.1 Baseline composite

The baseline carbon fiber composite is the Grafil 34-700 two-dimensional fiber weave fabric and the EPON 862 epoxy resin. The Grafil fiber weave and EPON epoxy are infused at a 50/50 weight fraction. Figure 10 shows the baseline composite.

Figure 10: Baseline composite

The resin is layered into a film in order to regulate the amount of resin. The layer of resin is sandwiched with one ply of the fiber weave and is cured in the autoclave. This same process is similarly repeated for the other composites.

2.4.2 CNT Composite

For this composite, CNTs (more specifically carbon nanofibers) are mixed into the resin prior to infusing with the Grafil weave. The CNTs are approximately 60 nanometers (nm) in diameter and 1000nm in length. Figure 11 shows the CNT composite.

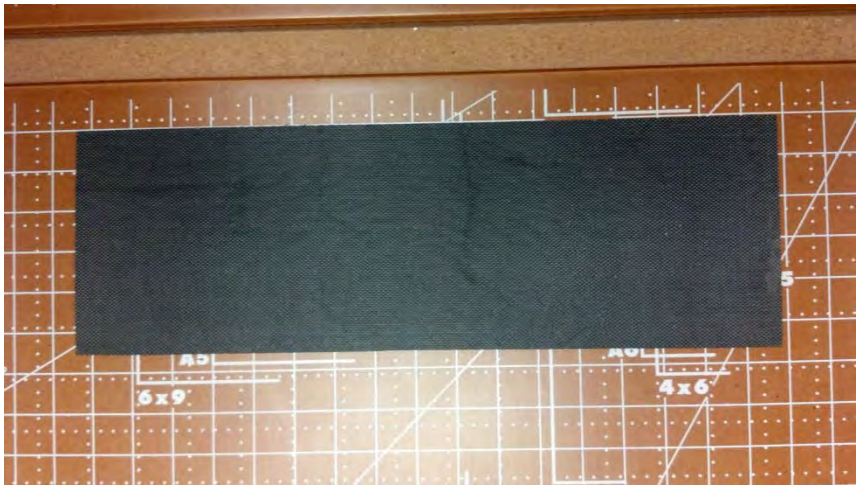

Figure 11: CNT composite

The CNT composite is made of 4% CNT, 46% resin, and 50% fiber weave by weight fraction. The CNTs are mixed into the resin uniformly using a paint mill to mix and layer into a film. The CNTs themselves are made from a process called chemical vapor disposition (CVD). The CVD process works to produce thin films or layers of high purity materials by chemical reaction of precursors and reactants. The CVD process is well understood and literature on the process is readily available. Each CVD process follows the same process but may differ in their "recipes." Specific information on the

CVD process used to produce the CNTs used in this research will not be discussed in additional detail.

The addition of CNTs in the composite is expected to improve both the mechanical and electrical properties. While this thesis will not determine the change mechanical properties of the tested materials, studies have been conducted to determine the effects of CNTs dispersed into resins. "The dispersion of the multi-walled CNTs in epoxy resin influences its strengthening effect," but also research has seen different composites "becoming more brittle with the incorporation of CNTs." [28] [29] Research has shown quality, type, size, resin, etc can change how the addition of CNTs affect the composites performance. Similar research shows this holds true for the electrical properties. Additional discussions on the electrical properties of carbon-based materials are in further sections.

2.4.3 Nickel Coated CNT Composite

Similarly as the CNT composite, Ni-coated CNTs are mixed in the resin before being infused to the fiber weave via the autoclave. The same CNTs go through a specific process to coat them with nickel. The process includes conditioning the CNTs in different solutions and adding reactants and precursors to produce the nickel coating. The thickness of the coating is regulated by the timing and chemical reactions among other things. The Ni-coated CNTs are mixed with the resin and the fiber weave in the same manner and ratio as the CNT composite. The CNTs in this research are coated with 30nm of nickel. Figure 12 shows the Ni-coated CNT composite.

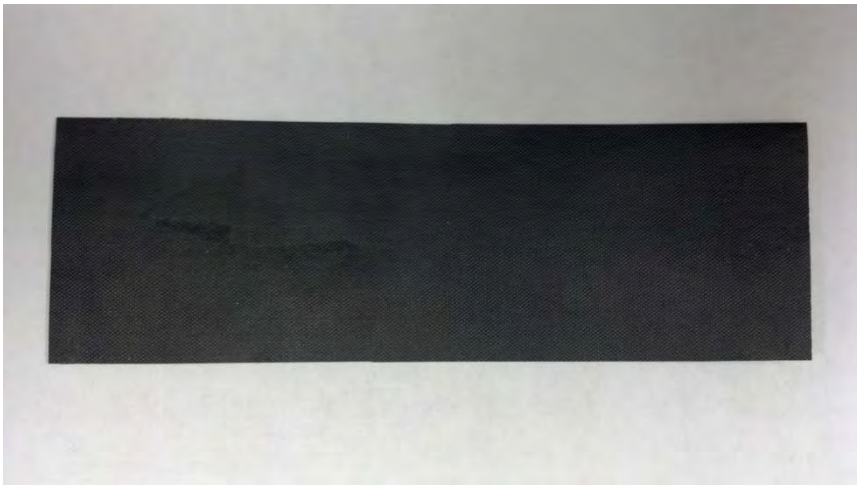

Figure 12: Ni-coated CNT composite

Similarly, the specific process used to coat the CNTs will not be discussed in any more detail. The nickel coating process information is proprietary.

2.4.4 P100 Carbon Fiber Composite

The P100 carbon fiber is commercially produced mesophase pitch high conductive fiber by a company called Amoco. Mesophase pitch describes the precursor used to create the continuous carbon fibers. This process works by melting down the mesophase pitch precursor into a thick liquid. The liquid is sprayed out of spinning jets where it is stretched to align the molecules in a fiber and remove voids. This fiber is subject to various gasses and temperatures. At the end of the process, the pitch (usually coal or oil based) is ultimately replaced with only carbon elements (carbon or graphite)

then surface treated. This is one of several ways to make carbon fiber. More information on the mesophase pitch process is available in published literature.

For the P100 fiber, not much public information is available. The fiber has a ultimate tensile strength of 970 MPa, tensile modulus of 470 GPa, and a density of 1.8 grams per cubic centimeter. The P100 fibers did not come in an already woven fabric. Instead, the fibers come as individual loose strands. To incorporate the fibers into the composite, they were hand aligned on a sheet of resin. The P100 fiber and EPON epoxy combined weight fraction was 50% of total weight. Figure 13 shows the P100 Composite.

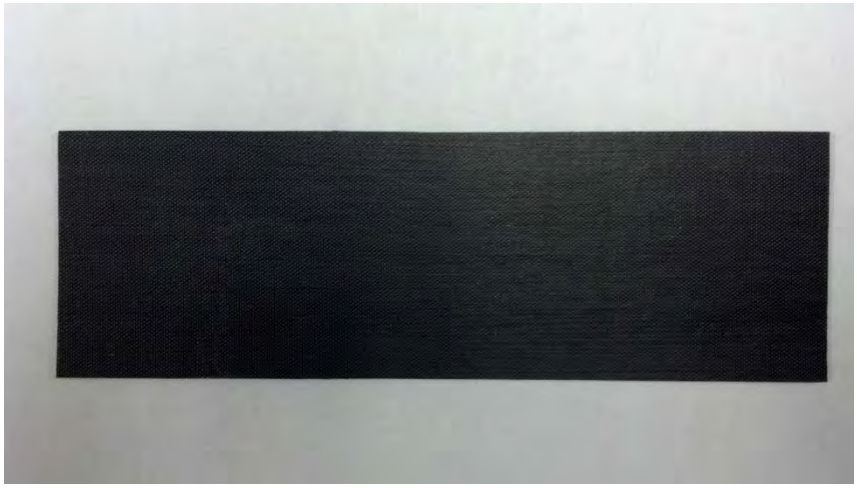

Figure 13: P100 Composite

2.4.5 Pyrolitic Graphite Composite

Pyrolitic graphite is highly aligned graphite produced using the CVD method. A substrate is subjected to precursors and reactants under high temperature and pressure. The pyrolitic graphite was made at 2200 degrees Celsius and a pressure of 133 Pa (1 torr). In the process, carbon is slowly deposited in thin layers across a substrate. The process is repeated

until the desired thickness is achieved. Once the pyrolitic graphite was produced, the EPON resin was used to adhere it to composite. Figure 14 is the pyrolitic graphite composite.

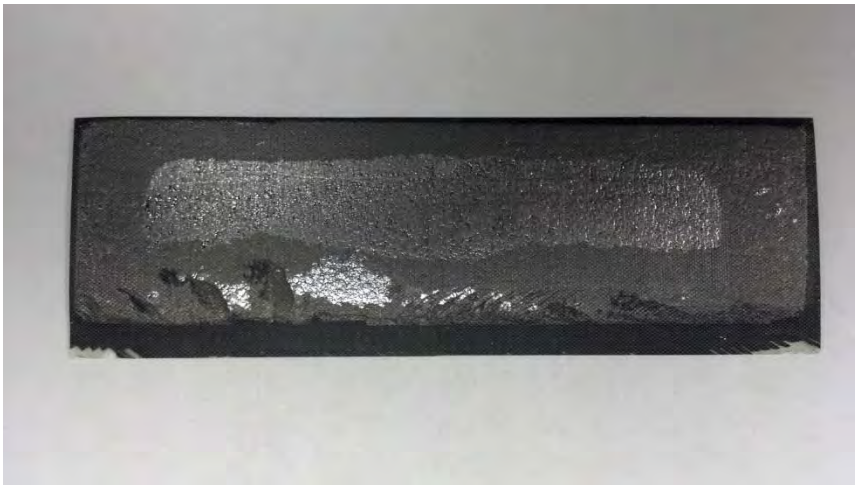

Figure 14: Pyrolitic graphite composite

Carbon based materials and the theory that effect their materials properties will be further discussed in the next sections. The purpose of this section was to introduce the materials.

2.5 Carbon based materials background

The inside material of rectangular hollow waveguides are almost extensively made of metals. The metals have a high conductivity and results in a very low energy loss as the wave propagates through the waveguide. This research focuses on alternative materials that would allow the waveguide to perform its function with minimal drop in performance. This section will describe different types of carbon based crystalline forms.

Graphene is “a planar allotrope of carbon where all the carbon atoms form covalent bonds in a single plane.” [7] Allotropes are elements made of the same atoms as each other that are structurally bonded differently. A single plane graphene can be used

to create other types of carbon allotropes such as carbon nanotubes (CNTs), bucky balls, or graphite. A carbon nanotube is cylindrically rolled piece of graphene with a large length to diameter ratio. Bucky balls (officially called Buckminsterfullerenes) are 60 carbon atoms formed into a spherical structure similar to the shape of a soccer ball. Graphite is layered sheets of graphene, Figure 15 shows a two-dimensional sheet of graphene and these different carbon allotropes formed from this two dimensional sheet.

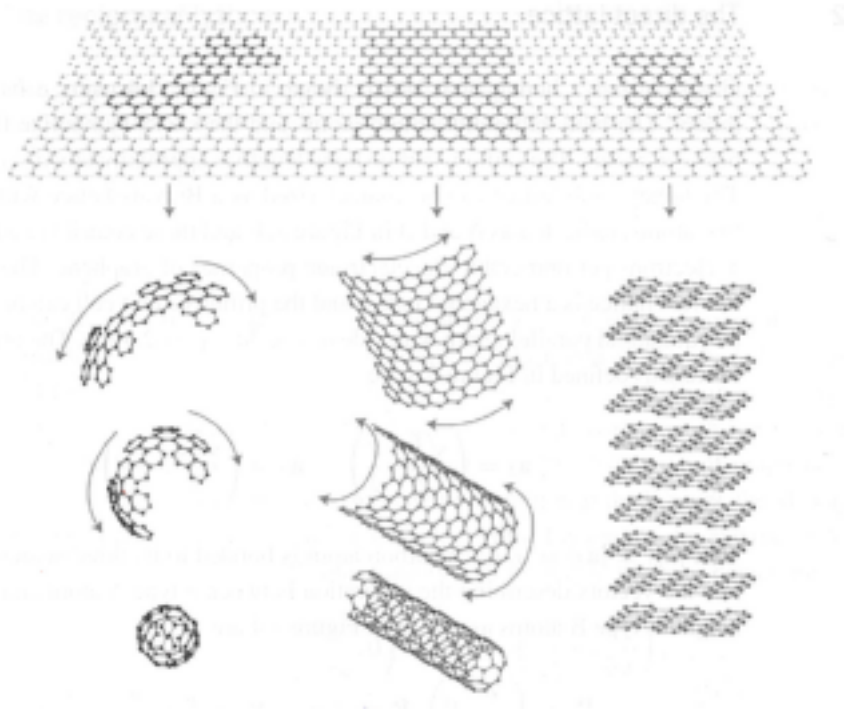

Figure 15: A graphene sheet being formed into bucky balls, CNTs, and graphite

The left side of Figure 10 depicts how a bucky ball is created out of a certain pattern of the graphene sheet. The center depicts how a CNT is formed and the right side shows how layers of graphene form graphite. This research will use and test CNTs and graphite.

Since graphene can be used to form other carbon allotropes, it is important to have a basic understanding of is atomic structure. A single carbon atom naturally has four valence electrons located in its second band, the P band. In graphene, the valence electrons from the carbon atoms will form three covalent bonds with neighboring carbon atoms and have the "electrons localized along the plane connecting carbon atoms." [7] These types of bonds are strong and responsible for the great strength and mechanical properties of graphene and CNTs. Normal to the plane or sheet formed by the carbon atoms, a much weaker type of covalent bonds is formed. Essentially, in a 2-D sheet of graphene, the carbon atoms in the same plane (the sheet) are strongly bonded together. These bonds do not require all the valence electrons. Therefore, the remaining electrons are loosely held normal the sheet. This is where the "electron cloud is distributed normal to the plane connecting atoms." [7] The electrons in these bonds are "weakly bound to the nuclei and, hence, are relatively delocalized.[7] These delocalized electrons are the ones responsible for the electronic properties of graphene and CNTs." [7] The delocalized electrons can become free electrons with little additional energy. The great mechanical strength of the carbon bonds and the delocalized electrons is what makes these carbon based materials warrant consideration for application in load bearing composite waveguides. They show the potential to handle the mechanical strength at lighter weight and posses the desired electrical properties (conductivity and permittivity).

CNTs can come in different types, and we will now distinguish them as either a single-walled carbon nanotube (SWCNT), a multi-walled carbon nanotube (MWCNT), or a graphene nanoribbon (GNR). A SWCNT is a hollow cylindrical structure of carbon atoms with a diameter that ranges from about .5 to 5 nm and lengths of the order of

micrometers to centimeters. A MWCNT is similar in structure to SWCNT but has multiple nested or concentric cylindrical walls with the spacing between the walls comparable to the interlayer spacing in graphite, approximately 0.34 nm." [7] For the different types of CNTs, we will focus on the electronic band structure derived from the band structure of graphene. This will give insight into the properties and performance of CNT devices. GNRs are discussed in more detail later in this chapter.

Chirality is an important concept used to "identify and describe different configuration of CNTs and their resulting electronic band structure." [7] A chiral object is an object whose mirror image is not superimposable onto itself. Objects whose mirror object can be superimposed onto its self are called achiral. All SWCNTs fall into one of these categories, which are broken down into further sub-categories. The physical structure of SWCNTs fall into either chiral, armchair, or zigzag lattice structure as depicted in Figure 16. The SWCNTs in Figure 16b and 16c, are achiral.

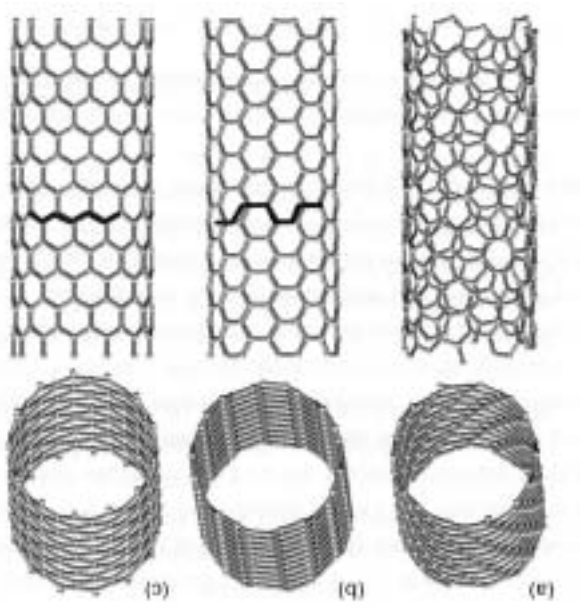

Figure 16: SWCNTs - (a) A chiral CNT, (b) armchair CNT, and (c) a zigzag CNT

A SWCNTs' chirality is important because it is a way of describing its electro-physical properties and gives insight to how a CNT will behave. SWCNTs, based on their chirality and diameter, can exhibit metallic or semiconducting properties. Their properties "vary in a predictable way from metallic to semiconducting with diameter and chirality." [24] All armchair SWCNTs are of the metallic type. "One out of three zigzag and chiral tubes show a very small band gap due to the curvature of the graphene sheet, while all other tubes are semiconducting with a band gap that scales approximately with the inverse of the SWCNTs radius." [7] Band gaps of 0.4 to 1 eV can be expected for some SWCNTs (corresponding to diameters between 0.6 and 1.6nm)." [24] These band gaps values fall between those typical of conductors and semiconductors as discussed in section 2.2. Researchers are looking into ways of manufacturing and separating metallic SWCNTs and/or their non-metallic counterparts.

MWCNTs do not fit into the same category as SWCNTs because of its multiple layers. The multiple layers and the proximity of the concentric tubes make all MWCNTs as a whole metallic. All the layers of a MWCNT contribute to its conductivity and large diameter MWCNTs have rather low resistance because MWCNTs posses a large number of conducting channels. [30] MWCNTs can be made to "have a negligible forbidden gap" depending on length, inner and outer diameters, and interlayer distances. [30]

This research will also look into graphene nanoribbons (GNRs). GNRs are a form of CNTs that are "narrow rectangles made of graphene with widths on the order of nanometers up to tens of nanometers" and are considered quasi one-dimensional. [7] GNRs are similarly categorized as SWCNTs in terms of being conducting,

semiconducting, armchair GNRs, and/or zigzag GNRs. GNRs differ from graphene sheets because of its small width and quasi one-dimensionality. Unlike an electrons ability to move two dimensionally in graphene sheets, GNRs have several factors (such as a quantum confinement and the boundary conditions at the edges) that differentiate the band structure compared to graphene. [7] Zigzag GNRs are semi-conductors with band gaps (forbidden gap) that are inversely proportional to the GNRs width. Armchair GNRs' band gap also depends inversely on width but also the carbon atoms on the edges. Experimentally, GNRs have shown to have a band gap of 0.2 to 1 eV, but as the GNR's width reach approximately 50 or 100 nm then the band structure returns to that of graphene. [25] [26]

2.6 Electromagnetic Material Properties Measurements

The electromagnetic properties, such as permittivity, are determined by collecting scatter (S) parameters. The S parameters are collected using an Agilent E8362B network analyzer connected to a hollow rectangular waveguide. The sample under test is placed between two sections of the waveguide. This test method is called the transmission reflection method (TRM). Once the S parameters are collected, the data is processed in MATLAB using the Nicolson-Ross-Weir (NRW) algorithm to produce different electromagnetic material properties. The following section will provide a basic understanding of each of these components used in this research.

The S parameters are derived from a two-port network whose input microwaves are labeled as a_i and the output microwaves are labeled b_i where i =1, 2. Figure 17 shows a nominal picture of a two-port network.

Figure 17: Two-port network with inputs labeled

The scattering [S] parameters are used to describe the relationship between the input [a] and output waves [b]:

$$[b] = [S][a] \tag{5}$$

Where [a] = [a1, a2] transposed and [b] = [b1, b2] transposed. The scattering [S] matrix takes the form of:

$$[S] = \begin{bmatrix} S_{11} & S_{12} \\ S_{21} & S_{22} \end{bmatrix} \tag{6}$$

The scattering parameters are experimentally gathered and used to calculate material parameters such as reflection and transmission coefficients, impedance, and admittance parameters to name a few. The scattering parameters are labeled such that the S_{11}value represent the signal received from port one and transmitted from port one. The S_{21} value represents the signal received at port two transmitted from port one. These are the two S parameters we are interested in.

A network analyzer is an important tool in microwave engineering because they are used to "analyze a wide variety of materials, components, circuits, and systems." [5] A network analyzer is made up of a signal source, signal separation devices, and signal detectors. The network analyzer is capable of measuring the two forward traveling (a_i) and the two reverse traveling waves (b_i) independently. These signals are used to generate the S parameters. Figure 18 shows the ports on the network analyzer.

Figure 18: Agilent network analyzer

In the transmission reflection method, the sample under test is placed into a segment of a transmission line. In this research, the transmission lines are hollow rectangular waveguides, as shown in Figure 19. The transmission lines are WR-90 waveguides. The WR-90 waveguide primarily operates in the 8.20-12.4 GHz, X-band, frequency range. The physical dimensions of the waveguide determine its operating frequency range. The WR-90 has an opening of 2.286 by 1.016 mm (.9" by .4") which forces a cutoff and maximum frequency of 6.557 and 13.114 GHz respectively.

Figure 19: WR-90 waveguide transmission line

The material under test is placed between two sections of WR-90 waveguides and is perpendicular to the initial direction of the propagating EM wave. As the wave hits the material under test, energy is reflected off the material and/or through the material. The amount of the energy reflected or transmitted can be determined by the reflection and transmission coefficients. The coefficients range between 1 and 0 and represent the percentage of the initial energy either reflected or transmitted, depending on the coefficient. These coefficients are a function of a materials electrical properties. For instance, a material with high conductivity and a low relative permittivity (~1) will reflect the EM wave. This is ideal for use in waveguides as there is little loss of energy to heat. As discussed previously, conductivity and permittivity depend on the atomic make up of a material, the forbidden gap between the valence and conduction bands, and the number of free electrons. Conductivity and permittivity directly affect the measured S parameters. The following section will develop the equations to determine the reflection

coefficient, transmission coefficient, and ultimately the relative permittivity. The relative permittivity will be used to predict the conduction losses of that material if made into a waveguide.

2.7 Nicholson-Ross-Weir (NWR) algorithm and the complex wave equation

In the 1970s, Nicolson, Ross, and Weir derived explicit formulas for the calculation of the relative complex permittivity and permeability, known as the NWR algorithm. [5] In the NWR algorithm, the reflection and transmission coefficients are expressed in terms of the S parameters. The NWR algorithm is used for "non-metal" materials or materials that allow some energy to transmit through. The reflection coefficient is given by

$$\Gamma = K \pm \sqrt{K^2 - 1} \tag{7}$$

with

$$K = \frac{S_{11}^2 - S_{21}^2 + 1}{2S_{11}} \tag{8}$$

in addition, the transmission coefficient is given by

$$T = \frac{S_{11} + S_{21} - \Gamma}{1 - (S_{11} + S_{21})\Gamma} \tag{9}$$

Knowing the reflection and transmission coefficients, the relative permeability and relative permittivity are respectively calculated from

$$\mu_r = \frac{1+\Gamma}{(1-\Gamma)\Lambda\sqrt{{}^{1}/_{\lambda_0^2} - {}^{1}/_{\lambda_c^2}}} \tag{10}$$

and

$$\varepsilon_r = \frac{\lambda_0^2}{\mu_r({}^{1}/_{\lambda_c^2} - {}^{1}/_{\Lambda^2})} \tag{11}$$

with

$$\frac{1}{\Lambda^2} = -\left[\frac{1}{2\pi D}\ln\frac{1}{T}\right]^2 \tag{12}$$

whereλ_o is the free-space wavelength, c is the speed of light (~$30 * 10^9$ cm/s), f is the frequency, and *D* is the thickness of the sample.

$$\lambda_o = \frac{c}{f} \tag{13}$$

λ_c is the cutoff wavelength of the waveguide (a function of a waveguides dimension)

$$\lambda_c = \frac{c}{f_c} \tag{14}$$

where

$$f_c = \frac{1}{2a\sqrt{\mu_0\varepsilon_0}} \tag{15}$$

where μ_0 is the free space permeability, and ε_0 is the free space permittivity.

For metals and metal like materials, the NWR algorithm does not allow us to determine the permittivity or permeability of the material. The NWR algorithm requires a component of the energy to transmit through the material,S_{21}. In reality, some energy is transmitted through the metal, but the network analyzer cannot distinguish such a weak

signal from normal noise. For materials with metal properties, we cannot determine its dielectric constant (permittivity) using this method. Instead, we use the complex field reflection and transmission coefficient.

$$Reflection\ Coefficient = \sqrt{S_{11}^{real\,2} + S_{11}^{imag\,2}} * e^{-\tan^{-1}\frac{S_{11}^{imag}}{S_{11}^{real}}} \quad (16)$$

$$Transmission\ Coefficient = \sqrt{S_{21}^{real\,2} + S_{21}^{imag\,2}} * e^{-\tan^{-1}\frac{S_{21}^{imag}}{S_{21}^{real}}} \quad (17)$$

In equations 16 and 17, the complex equation separates the magnitude of the coefficients. For example in equation 16, $\sqrt{S_{11}^{real\,2} + S_{11}^{imag\,2}}$ is the magnitude of the reflection coefficient. Ideally, this term will equal approximately negative one meaning that almost all the energy is reflected back. The $e^{-\tan^{-1}\frac{S_{11}^{imag}}{S_{11}^{real}}}$ term is the phase shift. As you can see, putting the reflection coefficient in this complex form allows the magnitude and incident angle to be easily separated. The coefficients can be converted to decibels (dB). For the dielectric coefficients, multiply the entire quantity by 20log10. For metals, you can convert the reflection coefficient into dB by multiplying the magnitude of the EM field, by 20log10.

2.8 Conduction (ohmic) losses

Using the S parameters to calculate a materials coefficients, permeability, and permittivity, we can compare a material's X-band RF performance. If we can determine the dielectric constant (permittivity) and measure the sheet resistivity, we can then

determine the total attenuation constant (losses) of a specific material if made into an X-band waveguide (as the lining). The total attenuation constant is

$$\alpha_t = \alpha_d + \alpha_c \tag{18}$$

with α_d being the dielectric attenuation and α_c being the conduction (ohmic) losses. The waveguide will be filled with air, not a dielectric material, therefore $\alpha_d = 0$. The conduction losses relate to the loss of electromagnetic energy on the waveguide's inner walls due to the materials resistance to the current imparted by the EM wave and governed by Maxwell's equations. Conduction losses are the primary focus of this research. This loss of energy is dissipated in the form of heat. Now the conduction (ohmic) losses are calculated as

$$\alpha_c = \frac{R_s}{\eta b} \frac{\left[1+\frac{2b}{a}\left(\frac{f_c}{f}\right)^2\right]}{\sqrt{1-\left(\frac{f_c}{f}\right)^2}} \tag{19}$$

where η is the intrinsic impedance of the material, which is the ratio of the electric and magnetic field within the material.

$$\eta = \sqrt{\frac{\mu}{\varepsilon}} \tag{20}$$

R_s is the sheet resistivity, measured using a 4-point probe, discussed more in a later section, and f is the frequency. The variables *a* and *b* (are the dimension of the waveguide as shown in Figure 20.

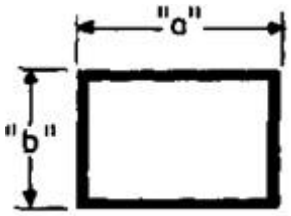

Figure 20: Hollow rectangular waveguide

The ohmic losses are calculated in Np/m. Equation 21 shows the conversion from Np/m to dB.

$$1\,\frac{\mathrm{dB}}{\mathrm{m}} = 8.686\,\frac{Np}{m} \tag{21}$$

Using the principles, algorithms, and equations discussed, we are able to determine the losses of a given material for the X-band frequency. This will allow comparing different materials, manufacturing process, resin, composites, etc and determining their suitability for use in antenna waveguide structures.

2.9 Statistical analysis

A sample size, *N*, of thirty or more random measurements ($\boldsymbol{x_i}$ where *i*=1,2,...,30) were taken for each sample. The standard deviation, s, and mean, $\overline{\boldsymbol{X}}$, for the sample set can be calculated and the results displayed at a specific confidence level using

$$\bar{X} - t\alpha_{/2}\left(\frac{s}{\sqrt{N}}\right) < z < \bar{X} + t\alpha_{/2}\left(\frac{s}{\sqrt{N}}\right) \tag{22}$$

where

$$s = \sqrt{\frac{\sum_0^{30}(x_i - \bar{X})^2}{N-1}} \tag{23}$$

From statistical charts, $t_{\alpha/2} = 1.96$ for a 95% confidence level and z is a point estimate (any data point in question). Equation (22) gives the data range where there is 95% confidence that any value of resistivity,z, will fall within that range. These equations and MATLAB will help determine some degree of accuracy of our measurements. [17]

2.10 Summary

This chapter described the basic theory and principles used to conduct the research in this thesis. A brief introduction to electromagnetic theory and Maxwell's equations was presented. This outlined the governing equations for EM waves. These theories and equations provided the boundary conditions used to develop the equations of how EM waves propagate through different types of materials and the basic effects. As electronic and magnetic components of EM wave radiates and interacts with a medium, Maxwell's equations state that the EM wave energy is transferred to the materials' electrons and nuclei. How the material reacts to the EM energy depends on the material electrical properties: conductivity, permittivity, and permeability.

Materials are categorized based on these properties as either conductors, semiconductors, or insulators. Why materials behave differently to EM waves depends on the principles of solid-state physics and the atomic structure of the material. This includes the number of free electrons, the size of the forbidden gap, and the bond structure between atoms to name a few.

More specifically, this thesis will research some carbon-based composites with films or layers made from different carbon allotropes. The chapter describes the atomic

structure and bonding of these materials that affect their mechanical and electrical properties.

The following sections describe the test methods used to determine the materials electrical properties. S parameters measured using a network analyzer and waveguide transmission lines provide use with the information to determine the material's electrical properties. Based on these calculated properties, we should be able to predict the materials electrical performance in a waveguide.

III. Methodology

This chapter will show the experimental process along with the laboratory equipment. Descriptions of the network analyzer, calibration process, and support equipment are provided. The network analyzer calibration process will be outlined and a description of the experiments is presented.

3.1 The low observable (LO) laboratory and support equipment

The AFIT LO laboratory specializes in testing materials and designs to determine their performance in the EM spectrum. The laboratory consists of several different types of equipment used to characterize materials and designs. This research utilized the labs Agilent E8362B network analyzer shown in Figure 21.

Figure 21: Agilent network analyzer

3.2 The network analyzer calibration process

The Agilent E8362B network analyzer's is capable of transmitting and receiving signals from 10 MHz to 20 GHz. The network analyzer must first be calibrated. Errors generally fall in three types of errors: drift, random errors, and systematic. Drift errors are caused by changes to the working conditions after calibration has been completed

such as temperature changes from when calibration occurred. Random errors are unpredictable and not fixed through calibration. These random errors can be from test repeatability, random noise, change in room temperature, moving the test cables, etc, and are minimized by averaging data from multiple measurements. Systematic errors are errors cause by the system from imperfections in the measurement system. For the most part, these do not vary and can be characterized during calibration and mathematically removed. Systematic errors are corrected by calibration by determining the errors from measurements of known standards. [5] The calibration processed used is the thru-reflect-line method discussed further below. It measures against three standards, one of which is the brass plate shown in Figure 22.

Figure 22: Brass calibration plate

Taking 12 different and independent measurements on known standards allows the system to solve for the 12 systematic error terms. [5] The following is the setup and

calibration process used to prepare the network analyzer for measurements. To conduct the S parameter measurements, the system must be set up with the appropriate coaxial cables. The coaxial cable transmits the signal between the network analyzer and the transmitters and receivers in the waveguide. Maury microwave 8944C38 coaxial cables are used.

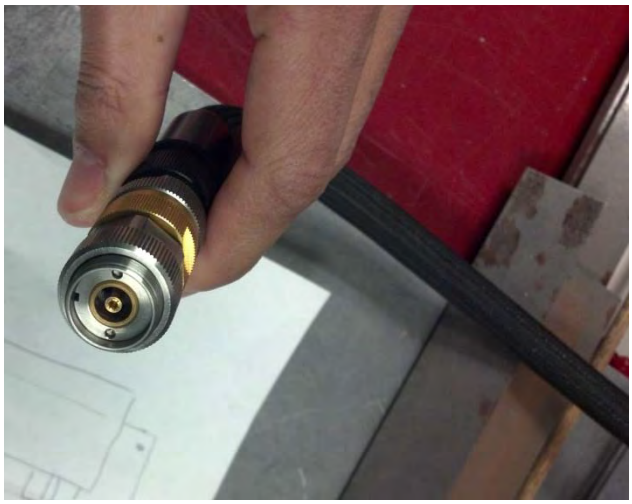

Figure 23: Coaxial cable connector

Torque wrenches are used to tighten the coaxial cables to the network analyzer. The torque wrenches, Figure 24, tighten the connectors between .9 to 1.36 Newton-meters (8 to12 in-lbs). They prevent the cables from being over torqued and damaging the connectors.

Figure 24: Torque wrenches

Using the same torque wrench, we attached the appropriate waveguide sections. To measure in the desired frequency range, we used a WR-90 waveguide model X103A5, as shown in Figure 25.

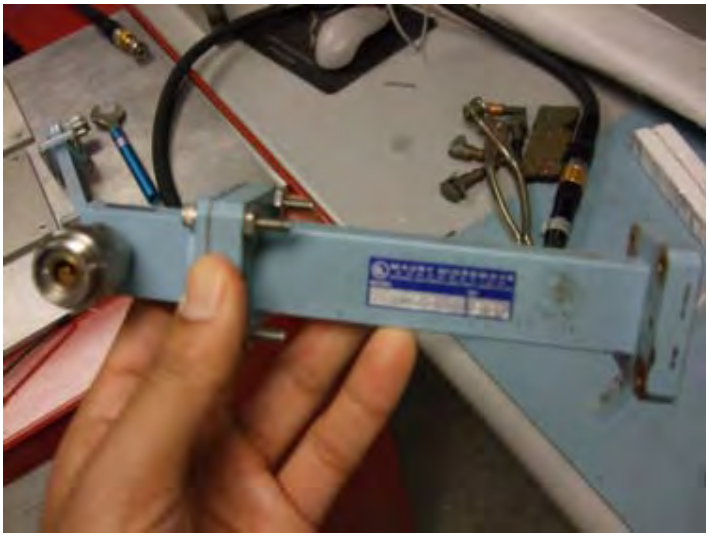

Figure 25: WR-90 waveguide section with coaxial connector

The next step in the calibration process is setting the network analyzer for a two-port calibration. The power is put on the network analyzer and one waits for the system to boot. The below steps were used to calibrate the system.

Setting up the network analyzer for calibration:

- Select “Channel” menu
  - “Start and Span”
    - 7-13 GHz (X-band)
- Select “Sweep” menu
  - Select “Number of Points”
    - Select appropriate number for resolution needed
      - Select 401 as a good default
  - Set “IF Bandwidth” to 50 Hz
  - Go to “Sweep setup”
    - Click Stepped Sweep box (put a check in it)
    - In Dwell time, set to appropriate time
      - Select 20 ms as a good default
        - This allows the system to be in a “steady state” before taking data
- Select “System” menu
  - Go to “Configure”
    - Select “System "Z_0"
      - Set to appropriate resistance
        - For rectangular waveguides, set to 1 ohm

These steps set the range at which data is to be collected, the number of data points to be collected, and at what frequency intervals the data is collected. The impedance, Z_0, is set to 1 ohm for rectangular waveguides. The setup process requires additional steps before the calibration is completed.

- Select “Calibration” menu
  - Clamp the 2 plates together and measure the thickness using the digital calipers
    - These plates become part of the waveguide, and the network analyzer needs to know the additional time it will take the waves to travel this additional distance.

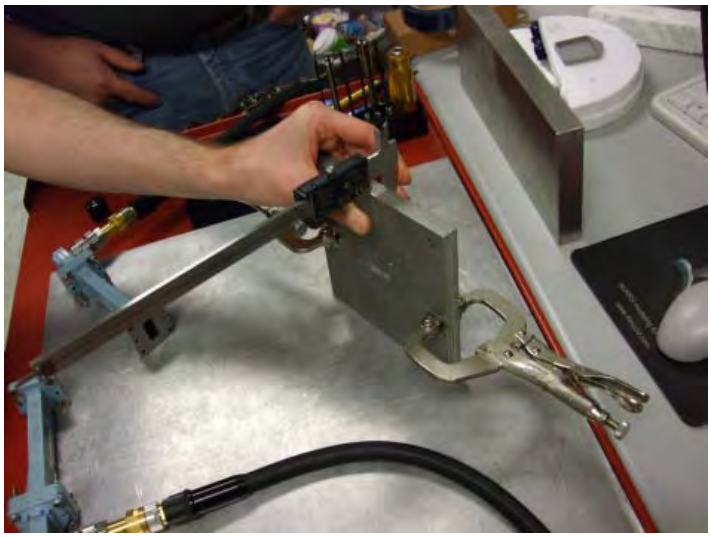

Figure 26: Metal mounting plates

- Select “Advanced modified cal kit”
  - Scroll and find “X clamp flange”
    - Click “edit kit”
      - Select “X band ¼ wavelength line
        - Click “edit”
          - Select “Delay characteristics”
            - Change to appropriate delay based on thickness of the two plates and speed of light
              - For plates pictured use negative 43.86367237 micro seconds
      - Select “Shorts”
        - Make sure all are zeros or ones
      - Select “Thru”
        - Make sure all are zeros and ones
      - Select OK
      - Select OK

These steps tell the system the type of calibration kit being used including the waveguide type and mounting bracket. The delay characteristic input comes from the additional length the EM wave has to travel from end to end (port a to port b) because of thickness

of the metal mounting plates. The thickness is multiplied by the speed of light to determine this time delay.

Once the system is setup for the calibration, you can begin to calibrate the network analyzer. The system is calibrated using the thru-reflect-line (TRL) two-port calibration technique. The TRL technique solves the 12 error terms and is primarily used in calibrating non-coaxial systems, such as waveguides. The biggest advantage of the TRL calibration method is that the required standards are easily designed, fabricated, and characterized. [5] To calibrate the network analyzer, the following was conducted.

Calibrating the network analyzer

- Select "Calibration" menu
  - Select "Cal wizard"
    - Click next
  - Click TRL
    - View select cal kit
      - Scroll and select "X clamp flange"
        - Click OK
      - Click next
    - Select "TRL ref plane"
      - Check box "Reflect standard"
      - Check box "System impedance"
      - Click next

Note: Try not to move the coaxial cables to max extent possible, as this would add systematic errors.

- Now measure "line standard"
  - This is with the wave guides together
  - Use guide pins to align the two waveguides
    - Clamp them together

Figure 27: Line standard measurement

- On the network analyzer, hit the green button that says “line”
  - Analyzer will measure until you see a check mark
- Now disconnect the wave guides

- Now measure “thru”
  - This is with the 2 plates in the wave guide

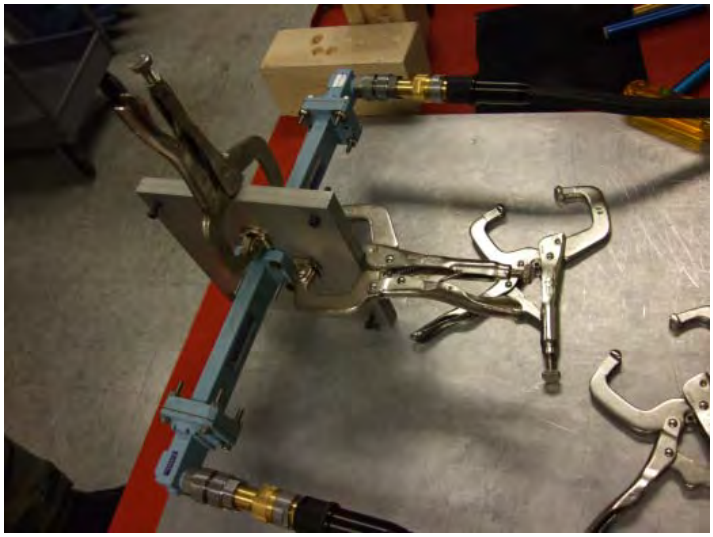

Figure 28: Thru measurement

- On the network analyzer, hit the green button that says “thru”

        - Analyzer will measure until you see a check mark
- Now measure “Short”
    - This is adding a brass plate between the two other plates

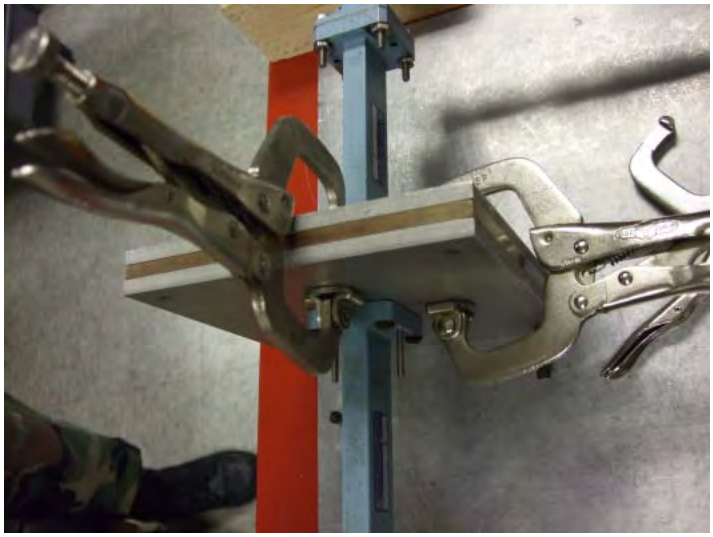

Figure 29: Short measurement with the brass plate between the two mounting plates

    - On the network analyzer, hit the green button that says “Short”
        - Analyzer will measure until you see a check mark
- Calibration is now complete

The TRL calibration technique measured multiple signal transmissions in the three different scenarios to solve the twelve error terms. First, it measures the output and input signals through just the waveguide fixture, then through the fixtures and mounting plates, then using a brass plate to short circuit the system. The system is now calibrated and ready to take S parameter measurements, but it is important to watch the test setup and procedure to ensure systematic errors are minimized. With the calibration complete, the system is ready for the samples. Figure 30 shows the two waveguide sections separated and the section between the two aluminum plates is where the sample under test is placed. For reference, port 1is the cable connected to the left waveguide section, and port

2 is connected to the right sections as shown in Figure 30. The S parameter S_{21} is the signal sent from port 1 to port 2 (or from left to right). The side of each sample that has the coating or film will be placed facing port 1, this will become more evident in later sections. This means we are focused on the waves traveling from port 1 to port 2, S_{21}, and the waves reflecting from port 1 back to port 1, S_{11}.

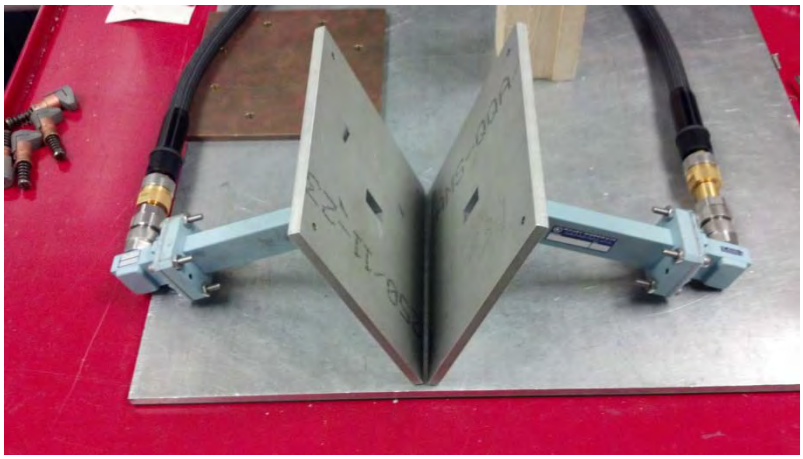

Figure 30: Test section

3.3 Transmission reflection method testing

Each sample material will be tested in random locations along the entire sample. Special caution is taken to ensure the area being tested is not within .5cm of the edges to minimize possible edge effects. The purpose is to measure different areas of the sample and gather multiple S parameter data sets. The multiple data sets will help ensure a certain degree in confidence in the data but also potentially give a little insight on how the variability in manufacturing across the sample may affect measurements.

The waveguide collects data on a 2.286 by 1.016 mm (.9" by .4") area of the material . This allows us to collect multiple data sets for each material. For example, Figure 31 shows the baseline sample.

Figure 31: Baseline composite

The sample is approximately 17 by 5 cm (7" by 2") and all samples are of similar size. In Figure 20, the sample is on a gridded table where each square is 1 cm by 1 cm. The thickness for each sample was collected at five different locations and varied by location. Table 1 are the measured thicknesses.

Table 1: Measured sample thicknesses

Measure Sample Thickness (mm)					
Measurement	Baseline	CNTs	Ni-coated CNTs	Pyrolitic Graphite	P100 fibers
1	0.79	0.75	1.27	1.67	1.23
2	0.81	0.66	1.21	1.76	1.34
3	0.76	0.86	1.13	1.75	1.29
4	0.79	0.72	1.25	1.77	1.25
5	0.75	0.74	1.09	1.82	1.3
Average	0.78	0.746	1.19	1.754	1.282

The thickness is used in the algorithms to process the data and determine the electrical properties for each sample. Figure 32 shows the baseline composite in the test setup.

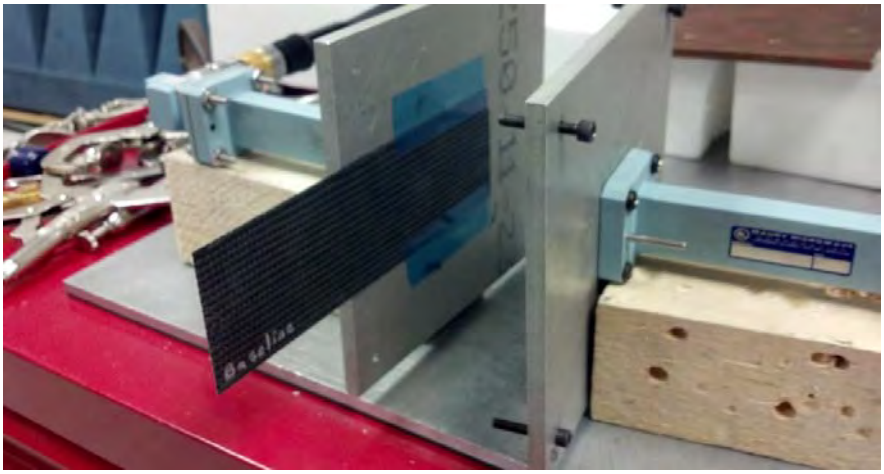

Figure 32: Baseline composite in the test section.

3.4 Testing the Materials

Once in the test section the two mounting plates are aligned together by four aligning screws (one in each corner), and the two sections are tightly clamped together. This allows the materials to sit flush against the opening in the two waveguide sections. Figures 33 shows the baseline composite ready for testing, and Figure 34 shows the P100 fiber composite ready for testing.

Figure 33: Baseline composite in testing

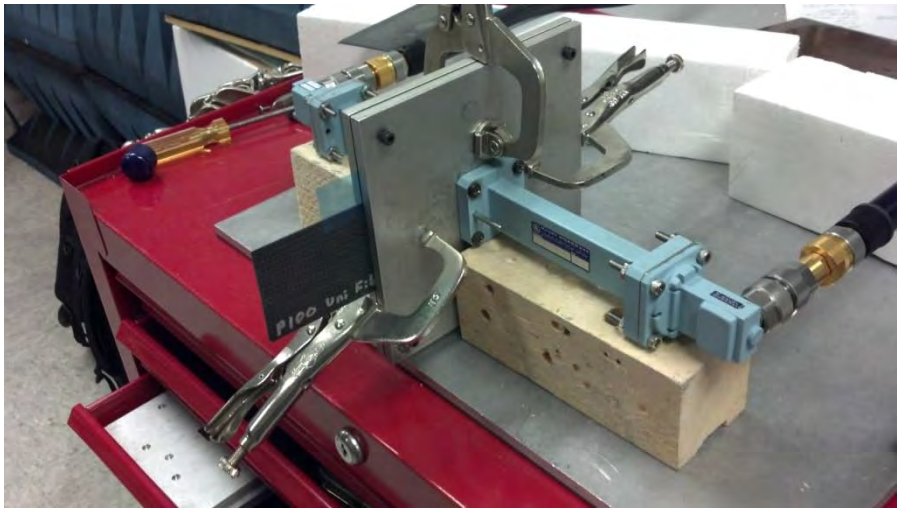

Figure 34: P100 fiber in testing

Once in the test section, the network analyzer conducts a sweep between the selected frequencies and records the data. This process is repeated 30-33 times at different sections on each sample. The data is then saved and transferred to a flash drive for data processing in MATLAB. For the purpose of this research it assumed there is not air gap between the material under test and the waveguide, this of course is not entirely true.

3.5 Resistivity Measurements

The surface resistivity measurement is conducted using the Guardian SRM-232 2000 and four point probe, shown in Figures 35 and 36.

Figure 35: Surface resistivity meter

Figure 36: 4 point probe

The four point probe is capable of resistivity measurements within 0 to 2000 ohms per square with a resolution of .8 ohms per square and an accuracy of 1.4 ohms per square at 1000 ohms per square. When taking the resistivity measurements, special care was taken to ensure the samples were not placed on metal. The metal would have changed to the measurement reading by providing a less resistive conduit for electrons to move through. The samples were placed on a foam block. Measurements were also conducted in certain material orientations because of the physical makeup of the material. Table 2 is the measured resistivity values for the composite materials.

Table 2: Resistivity measurements for the composite materials

Measure Sheet Resistivities (ohms per square)				
Baseline	CNTs	Ni-coated CNTs	Pyrolitic Graphite	P100 fibers
No value	No value	0-18	0	No value

Resistivity measurements for the baseline, CNT, and P100 fibers could not be collected because their resistivities were too high to measure. The samples were also sanded using 1000 grit sand paper to smooth the surface for the four-point but with no results.

IV. Results and Analysis

This chapter is broken down into the several parts of the experiments to meet the thesis objectives. Within each of these sections will be the recorded results and analysis. For all samples, data was collected between a frequency range of 7-13 GHz, do note the X-band range is approximately 8.2-12.4 GHZ. Also between 30-33 samples were collected for all composite materials. This was to ensure an adequate number of samples were taken over the entire sample to have a better representation of the data due to any number of different variables. However, not all these data are used due to errors. This helps reduce errors in data collection and allows us to try to calculate permittivity with a degree of confidence. Permeability for these materials is assumed and should be calculated to be about one with the exception of the nickel-coated CNTs. Nickel is a ferrous materials and has a relative permeability higher than one. Individual runs of data will not be labeled in the graphs as we are more concerned with the trend in the data, but individual data sets will also be presented.

4.1 Permittivity from NRW algorithm

The complex permittivity for each material was calculated using the NRW algorithm with questionable results. The results of the permittivity were found to be inconsistent and not possible across the different materials. The following Figure 37 shows the results using the NRW algorithm to calculate the imaginary part of the permittivity from the first five data sets of the baseline composite.

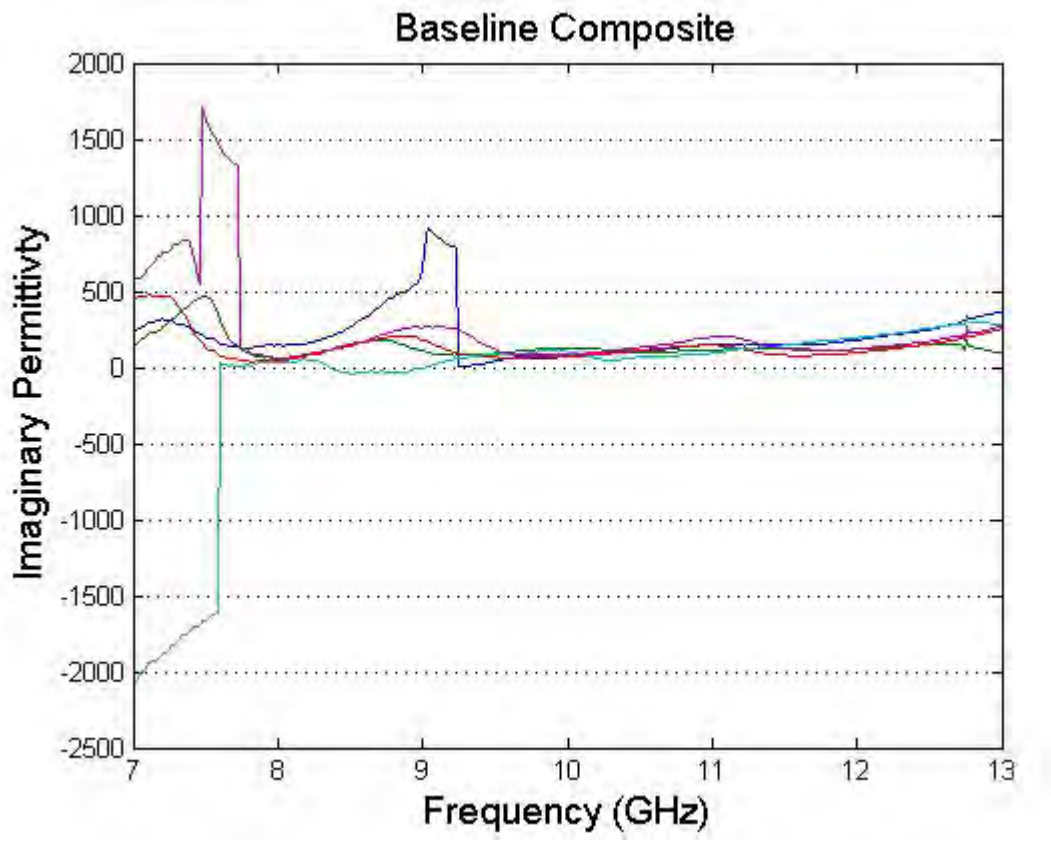

Figure 37: Baseline composite imaginary permittivity (runs 1-5)

The imaginary part of the permittivity should be a negative number as this relates to the dielectric losses in the material. In addition, the permeability is calculated as a check to ensure the data is correct. For nonferrous materials, the permeability should be approximately that of free space; therefore in terms of relative permeability, be equal to one. Figure 38 shows the permeability calculated by the NRW algorithm for the baseline configuration's first five data sets.

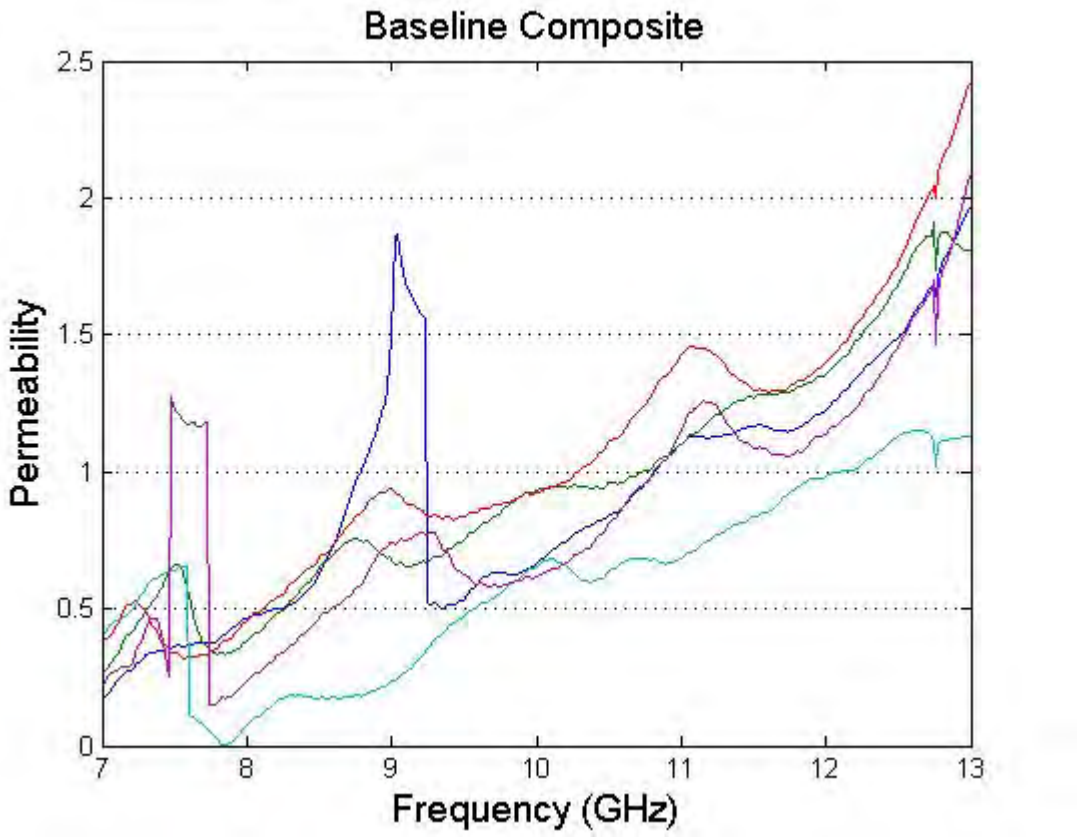

Figure 38: Baseline composite permeability (runs 1-5)

The permeability values are not as expected which means something is not correct in our data, test setup, assumptions, or algorithms.

4.2 Transmission and reflection coefficient

Upon inspection of the S_{21} parameter, it is observed that energy does not transmit through the material from port 1 to 2 on the network analyzer. Figure 39 shows S_{21} for the first five measurements of the baseline composite.

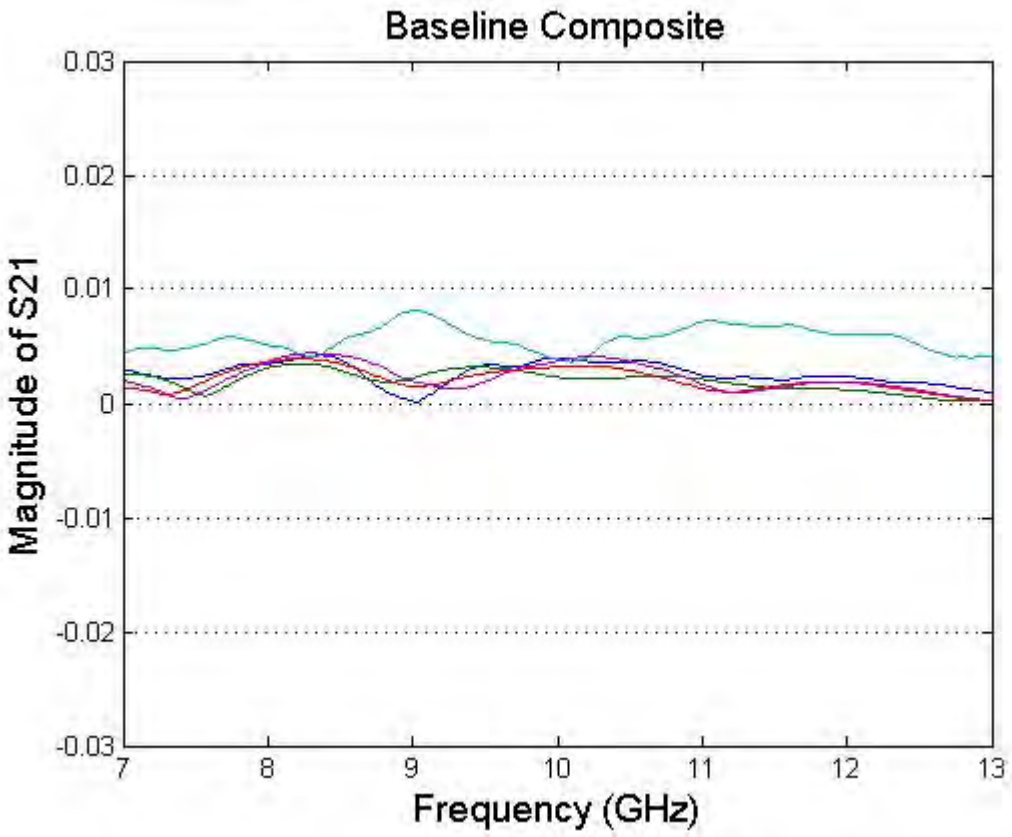

Figure 39: Magnitude of S_{21} for the baseline composite (runs 1-5)

The magnitude of the S_{21} parameter represents the transmission of the electric field through the composite, the transmission coefficient. In Figure 39, the S_{21} value is approximately zero. This concludes that energy is not transmitting through the material (at least not measureable amounts with the equipment). This becomes an issue when trying to use the NRW algorithm. The NRW algorithm requires two equations (S_{11} and S_{21}) to solve for permittivity and permeability. To verify energy is not transmitting through the material, we will look at the magnitude of the S_{11} parameter, which is the reflection coefficient.

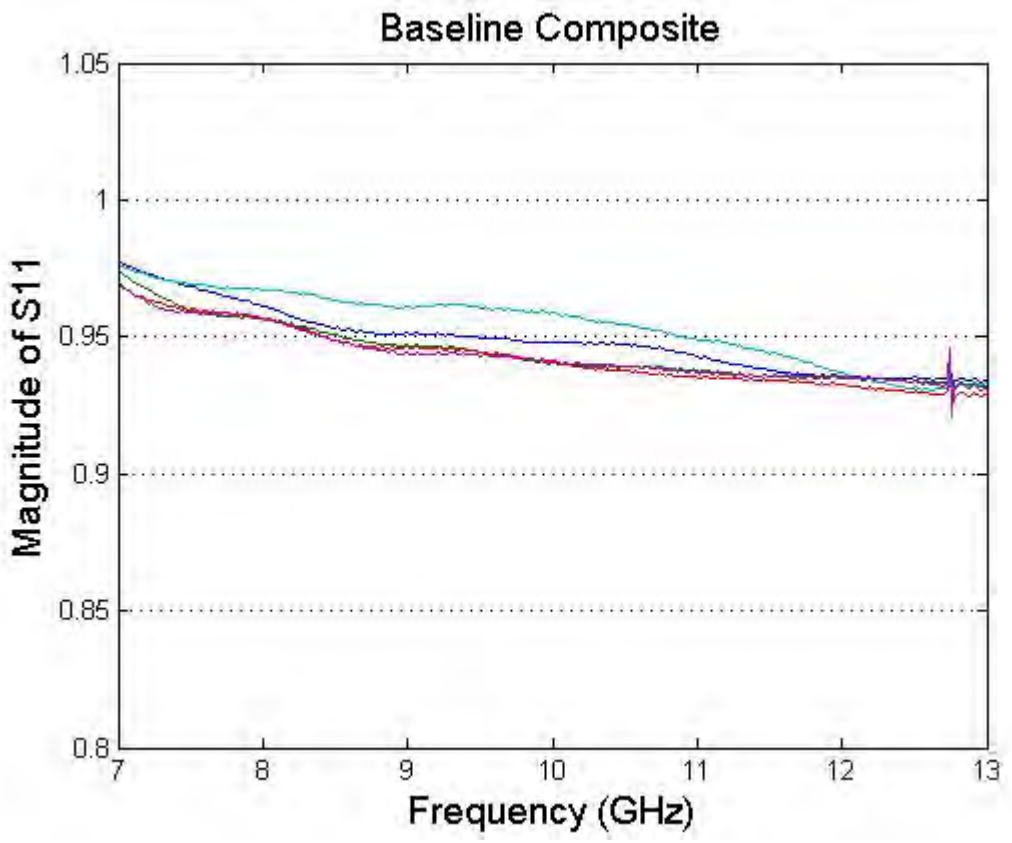

Figure 40: Magnitude of S_{11} for the baseline composite (runs 1-5)

It is shown in the figure that the reflection coefficient is relatively near one. This indicates most of the energy reflects off the sample. A closer examination of a data set will show that not all the energy is reflected or transmitted. Figure 40 shows the transmission and reflection coefficient for the same measurement or data set. At 10 GHz, the reflection coefficient is calculated at .9481, and the transmission coefficient is .00399. The reflection and transmission coefficients would add to 1 in a no loss scenario in which all the energy is either transmitted or reflected. In the case of the measurements in this thesis, it is expected energy is lost in the form of heat in the material under test. Other

potential losses are due to the aluminum walls in the WR-90 waveguides, but these are assumed perfect electrical conductors and therefore have negligible losses.

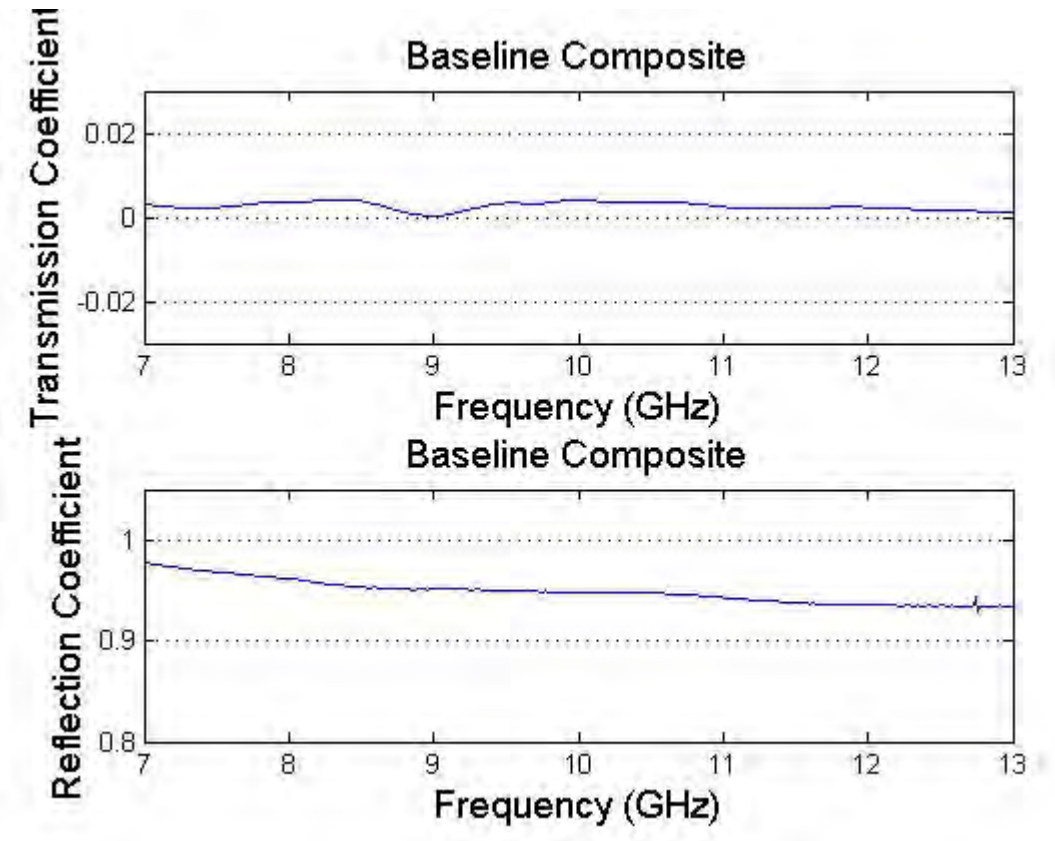

Figure 41: Transmission and reflection coefficient for one measurement

4.3 Power coefficients

From the reflection coefficients, you can determine the power coefficient of reflection. The power coefficient is the amount of power lost at reflection and can be easily calculated as the square of the reflection coefficient, magnitude of S_{11}. We will use this term to determine which material is best suited to most efficiently reflect X-band electromagnetic energy.

4.3.1 Brass Plate

The brass plate was used for calibration and represents a perfect electrically conducting material to the network analyzer. In the Figure 42, the brass plate will have a power coefficient of one. This indicates it reflects all power back. While we know this is not possible because of losses, we still consider it as perfect reflector of the EM energy. The network analyzer and S parameter measurements do not have the resolution to distinguish between the brass plate and one of copper or silver where would be silver the superior reflector in this application.

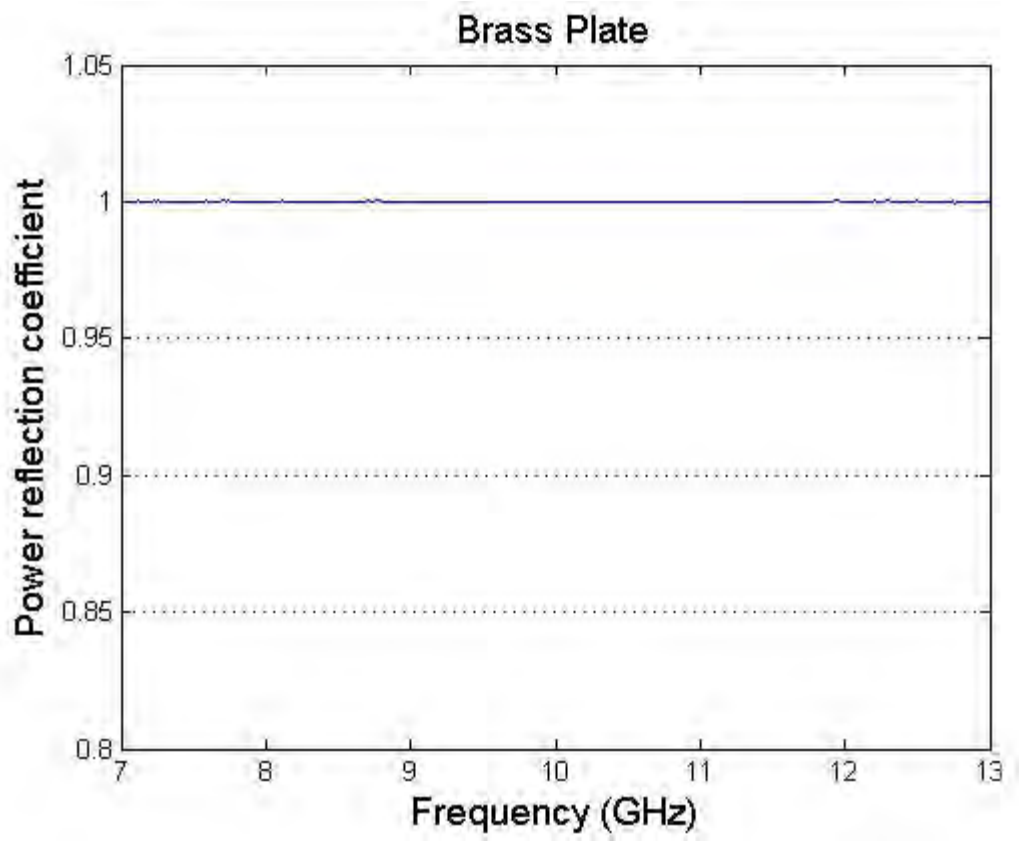

Figure 42: Power coefficient for the brass plate

Figure 43 is the brass plate's power coefficient at a zoomed in scale. Notice the power coefficient is within a thousandth of a percent of one (within the expected noise). This means almost all the power is reflected. Notice it is a positive 1 and does not show direction of the reflected power.

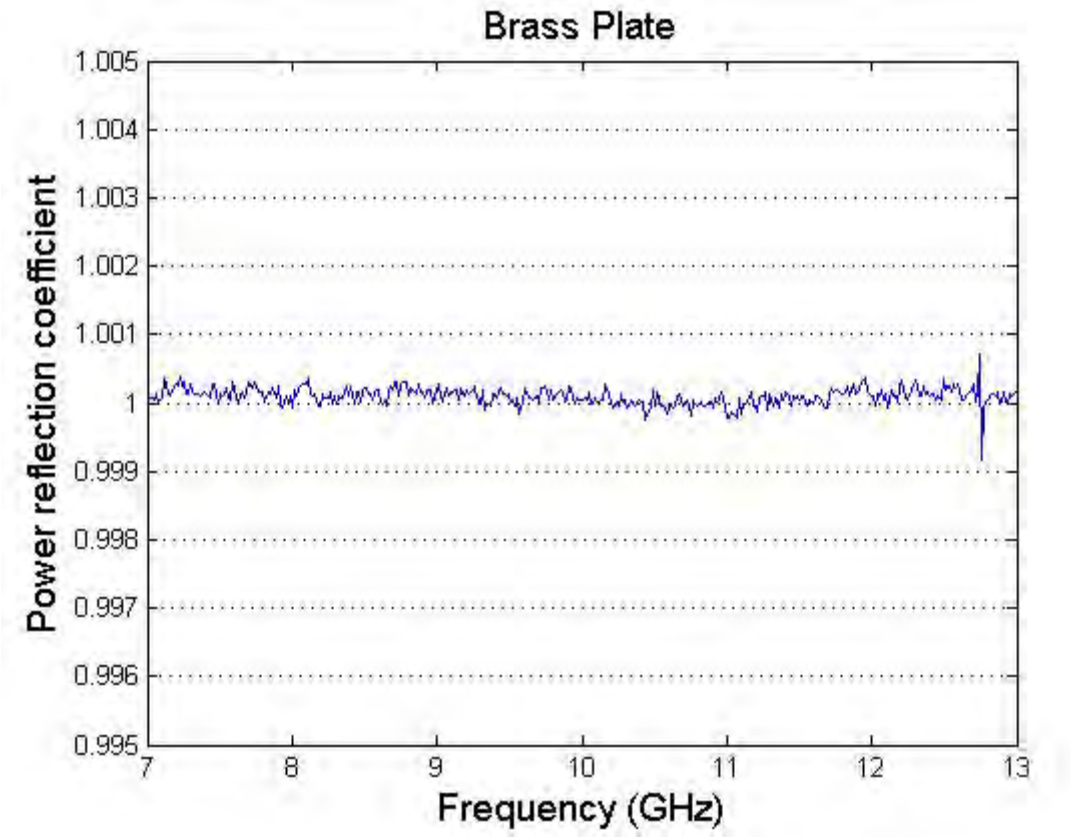

Figure 43: Power coefficient for the brass plate (magnified)

In addition, there is very little phase shift (or dielectric losses) with the brass plate. Figure 44 is the imaginary part of the reflection coefficient and represents the change in phase angle of the reflected wave. It is within a 1/1000th of a percent to zero meaning there is a -180 degree shift in the phase angle as it is reflected.

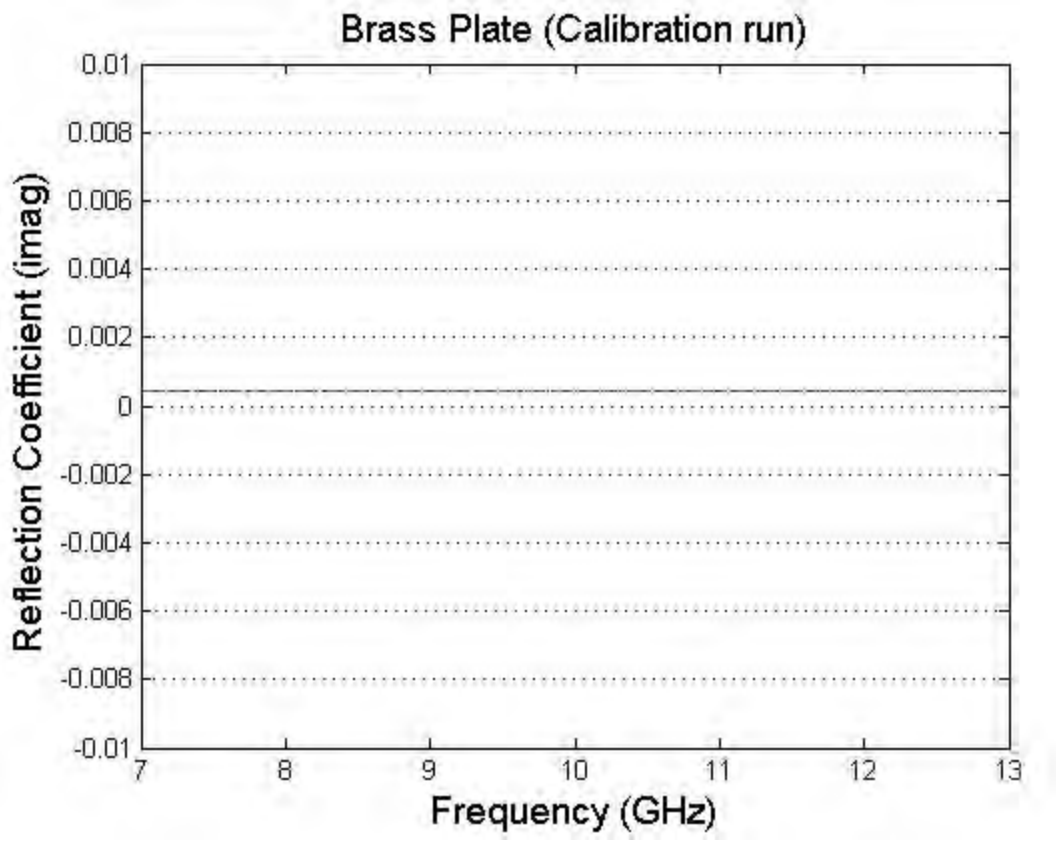

Figure 44: Imaginary part of the reflection coefficient

4.3.2 Baseline composite

Figure 45 shows the calculated power coefficient for the baseline composite. Each line represents 1 of the 33 measurements collected.

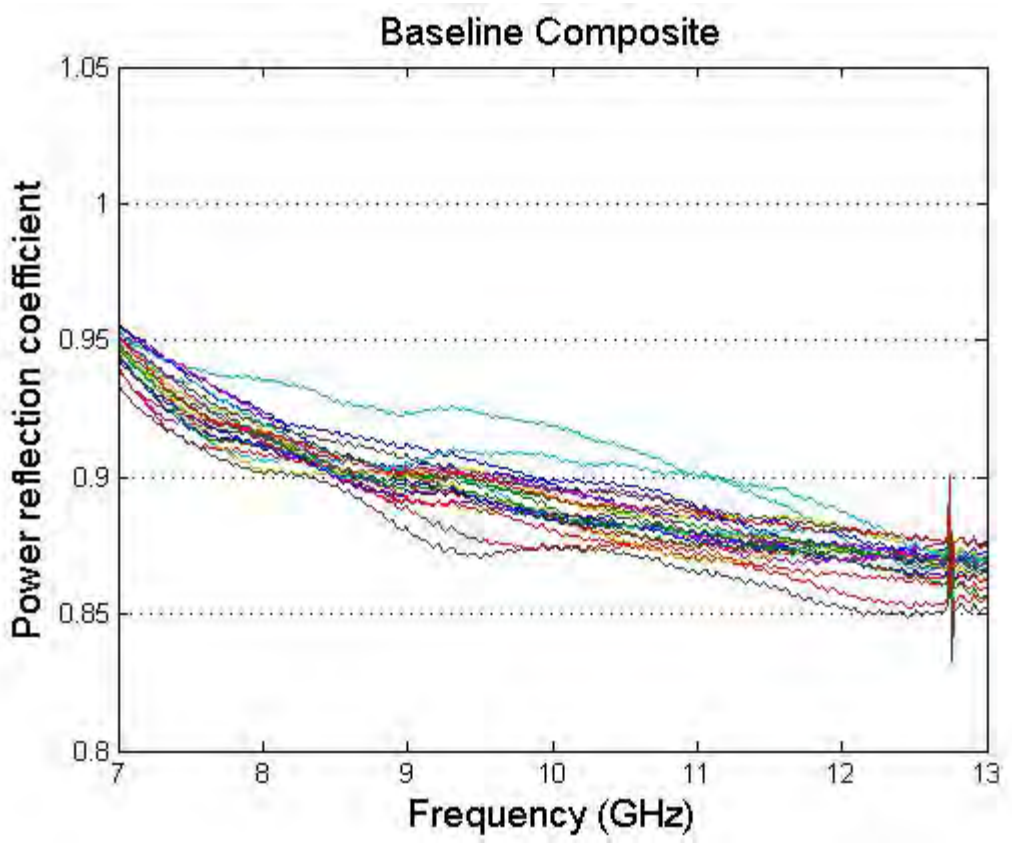

Figure 45: Power coefficient for the baseline composite

With the baseline composite, you see a drop in performance compared to the brass plate. The power coefficient is between 87.43-91.9% at 10 GHz and steadily decreases as the frequency increases. Figure 46 is the trend line calculated from Figure 44 above. The trend line is calculated as a quadratic polynomial. At 10 GHz, the power coefficient on the trend line is 89.2%.

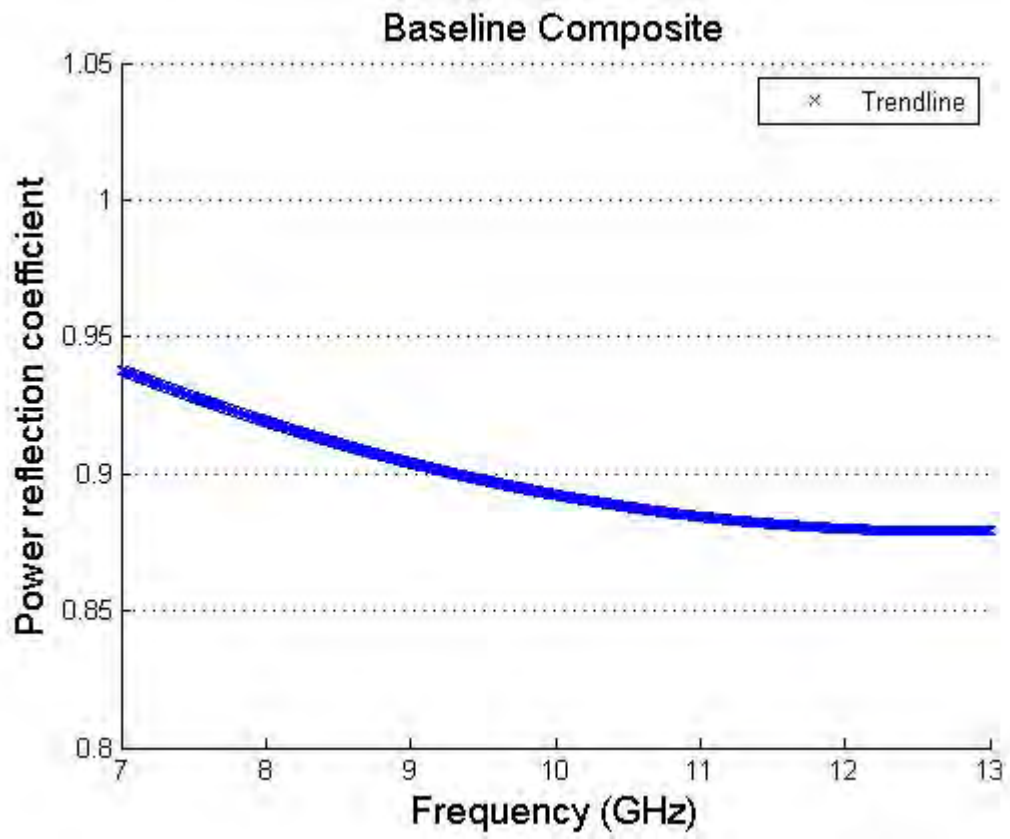

Figure 46: Power coefficient trend line for the baseline composite

These data will be analyzed and compared to the similar data from the other materials and allow a fair comparison among the different composites. Figure 47 shows the calculated power coefficient for the CNT infuse composite. Each line represents 1 of 33 measurements collected for this sample.

4.3.3 CNT Composite

Figure 47 shows the calculated power coefficient for the CNT infused composite. Each line represents 1 of 33 measurements collected for this sample.

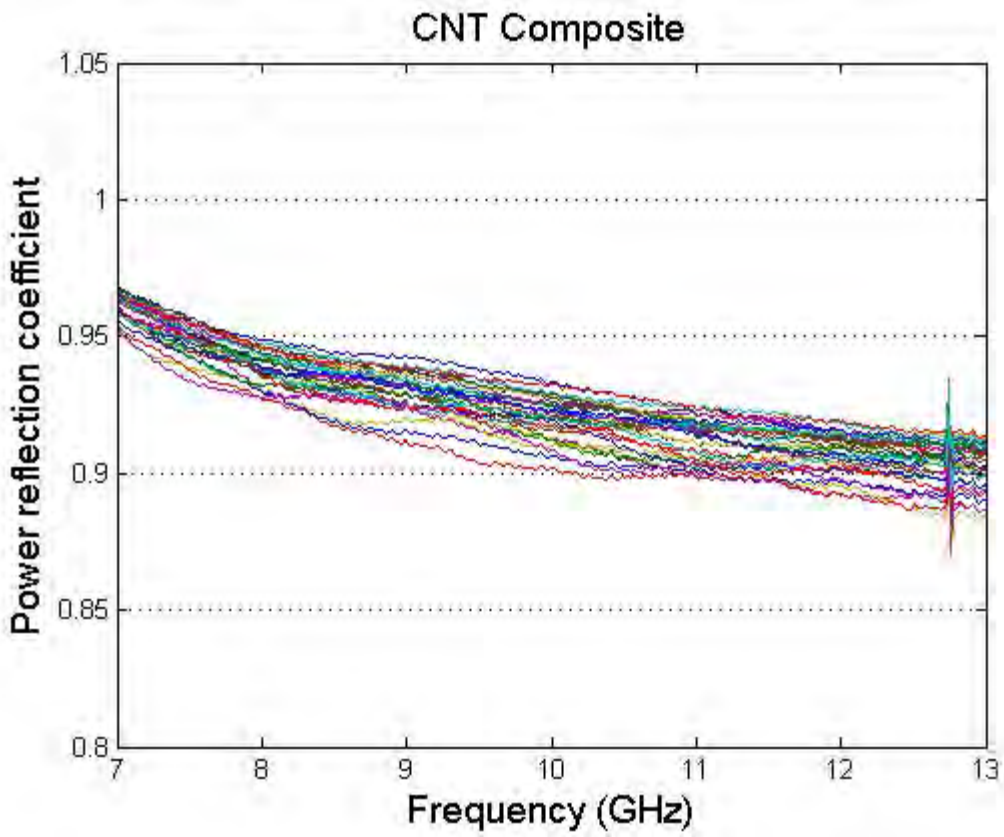

Figure 47: Power coefficient for the CNT composite

With the CNT composite, the power coefficient falls between 90.17-93.25% power coefficient at the 10 GHz frequency and steadily decreases as the frequency increases. Figure 48 is the trend line calculated from Figure 47 above. The trend line is calculated as a quadratic polynomial. At 10 GHz, the power coefficient is 91.51%.

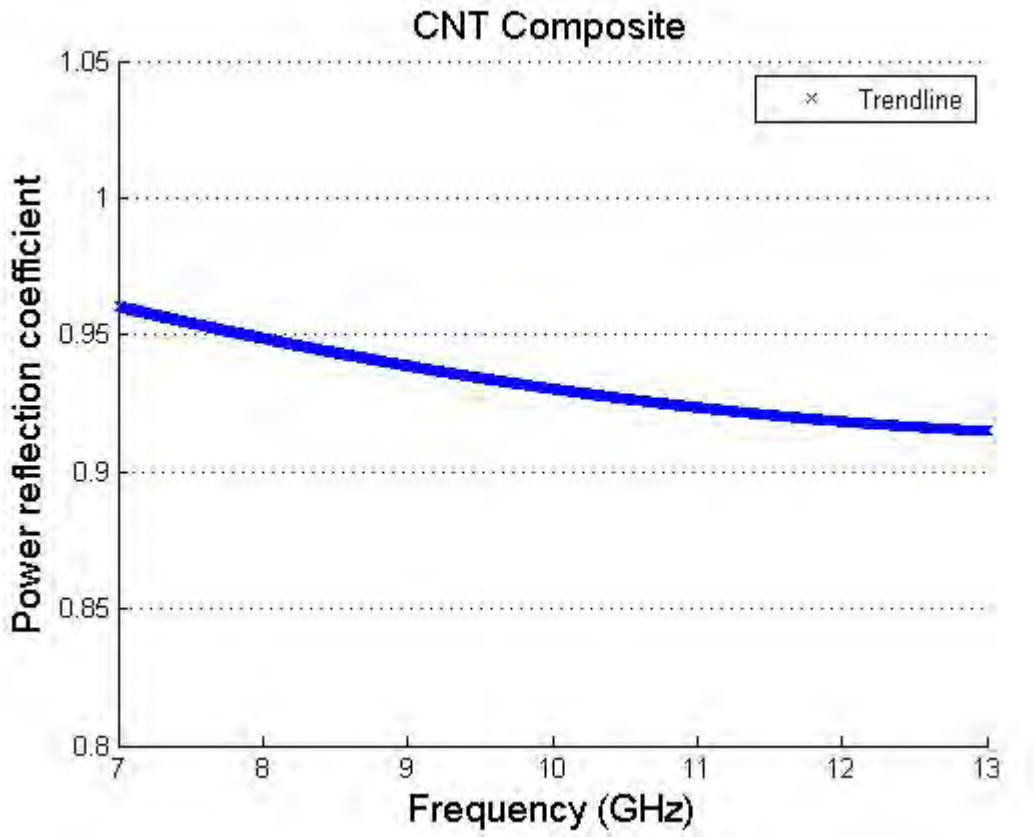

Figure 48: Power coefficient trend line for the CNT composite

4.3.4 Nickel coated CNT Composite

Figure 49 shows the calculated power coefficient for the Nickel coated CNT infused composite. Each line represents 1 of the 31 measurements collected.

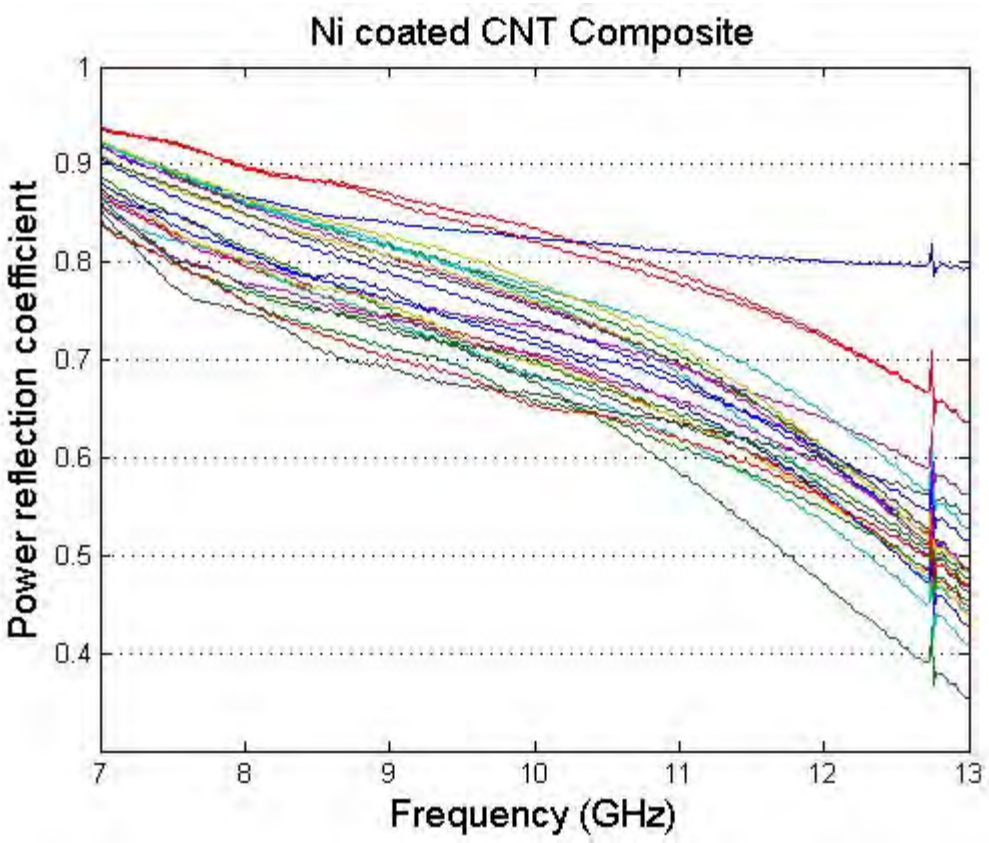

Figure 49: Power coefficient for the Nickel coated CNT composite

With the Ni-coated CNT composite, the power coefficient falls between 65.41-83.50% power coefficient at the 10 GHz frequency and steadily decreases as the frequency increases. Figure 50 is the trend line calculated from Figure 49 above. The trend line is calculated as a quadratic polynomial. At 10 GHz, the power coefficient is 91.51%.

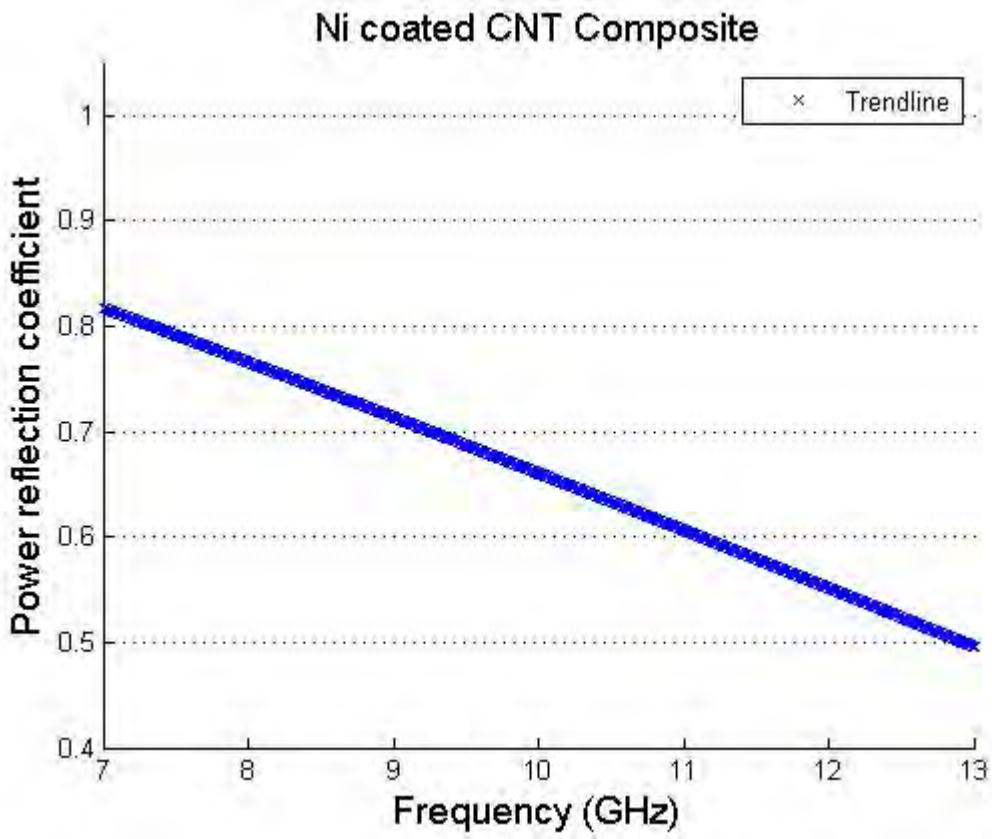

Figure 50: Power coefficient trend line for the Nickel coated CNT composite

4.3.5 P100 Fiber Composite

Figure 51 shows the calculated power coefficient for the P100 fiber composite. Each line represents 1 of the 32 measurements collected.

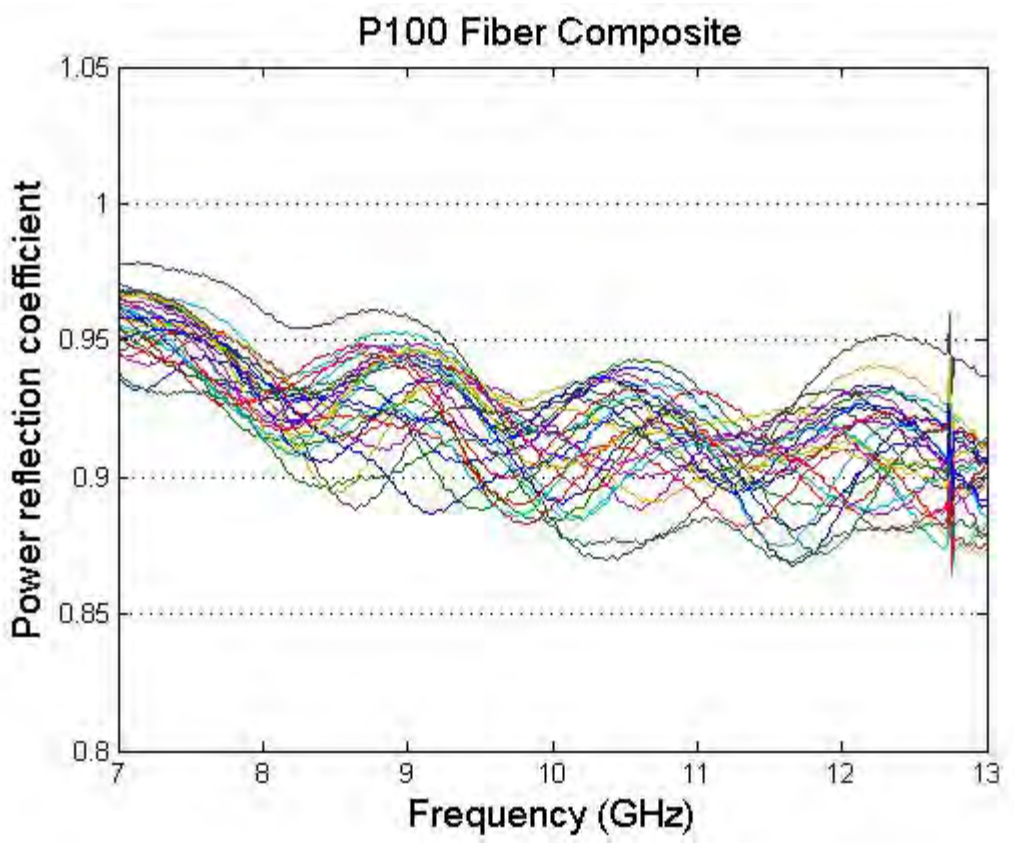

Figure 51: Power coefficient for the P100 fiber composite

The P100 fiber's measurements is quite different from the other composites in that the power reflection coefficient data in Figure 51 follow a periodic/sinusoidal type pattern. In analyzing the data, many of the data runs seem to consistently valley and peak at the same frequencies. The reason may be the wavelengths at these frequencies and the geometric alignment of the fibers. The spacing or physical dimension of the composite

surface may be some factor of the wavelengths at those frequencies. The power coefficient falls between 88.22-93.20% power coefficient at the 10 GHz frequency and steadily decreases as the frequency increases. Figure 52 is the trend line calculated from Figure 50 above. The trend line is calculated as a quadratic polynomial. At 10 GHz, the power coefficient is 90.34%.

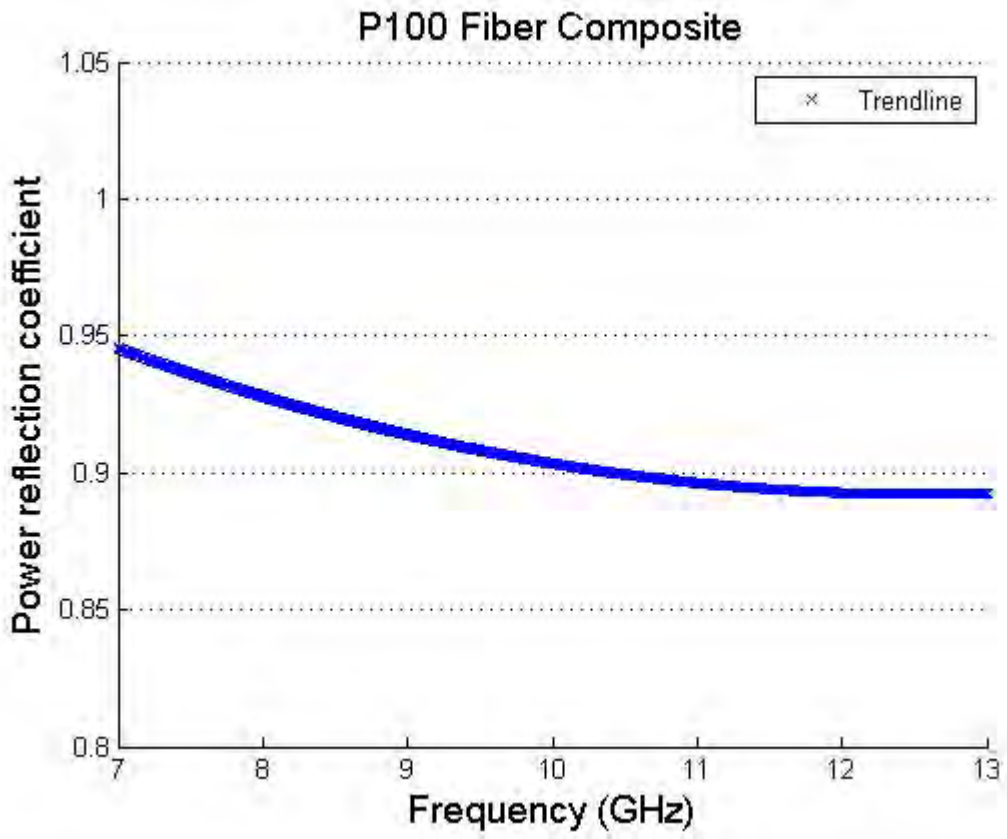

Figure 52: Power coefficient trend line for the P100 composite

4.3.6 Pyrolitic graphite

Figure 53 shows the calculated power coefficient for the pyrolitic graphite composite. Each line represents 1 of the 5 measurements collected.

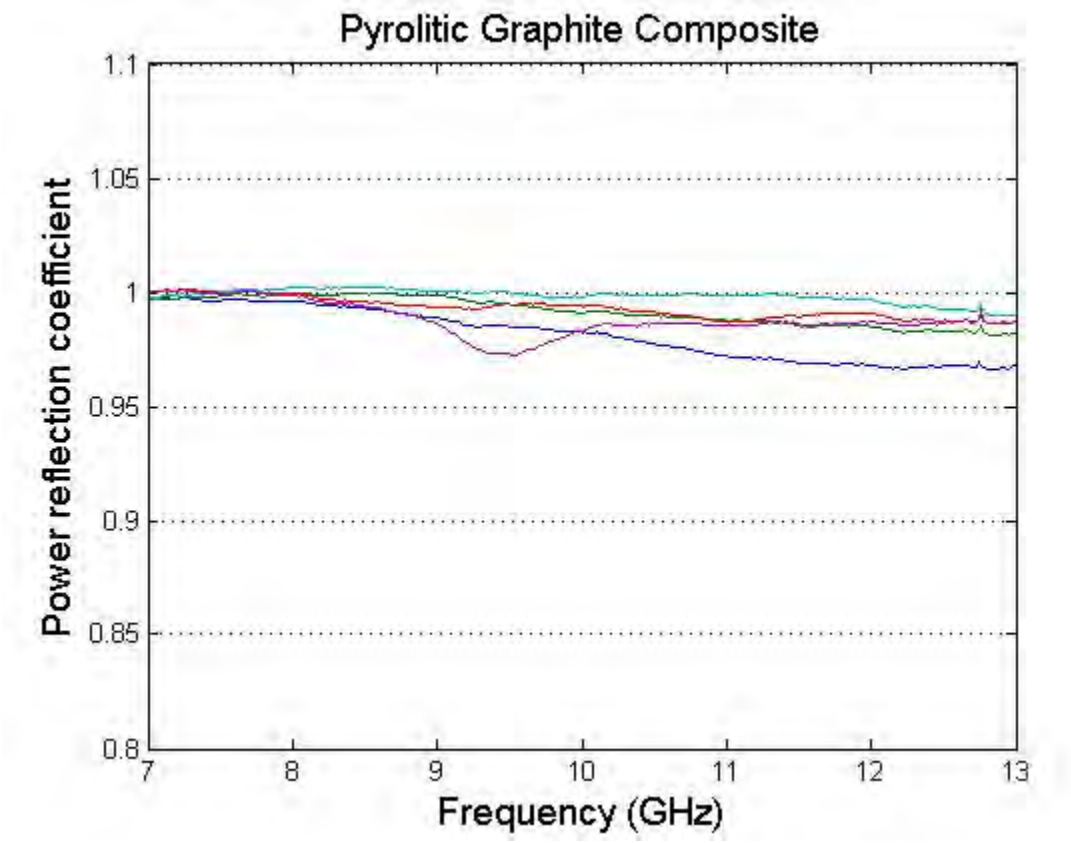

Figure 53: Power coefficient for the pyrolitic graphite fiber composite

With the pyrolitic graphite composite, the power coefficient falls between 98.32-99.82% power coefficient at the 10 GHz frequency and generally stays level as the frequency increases. Figure 48 is the trend line calculated from Figure 47 above. The trend line is calculated as a quadratic polynomial. At 10 GHz, the power coefficient is 98.82%.

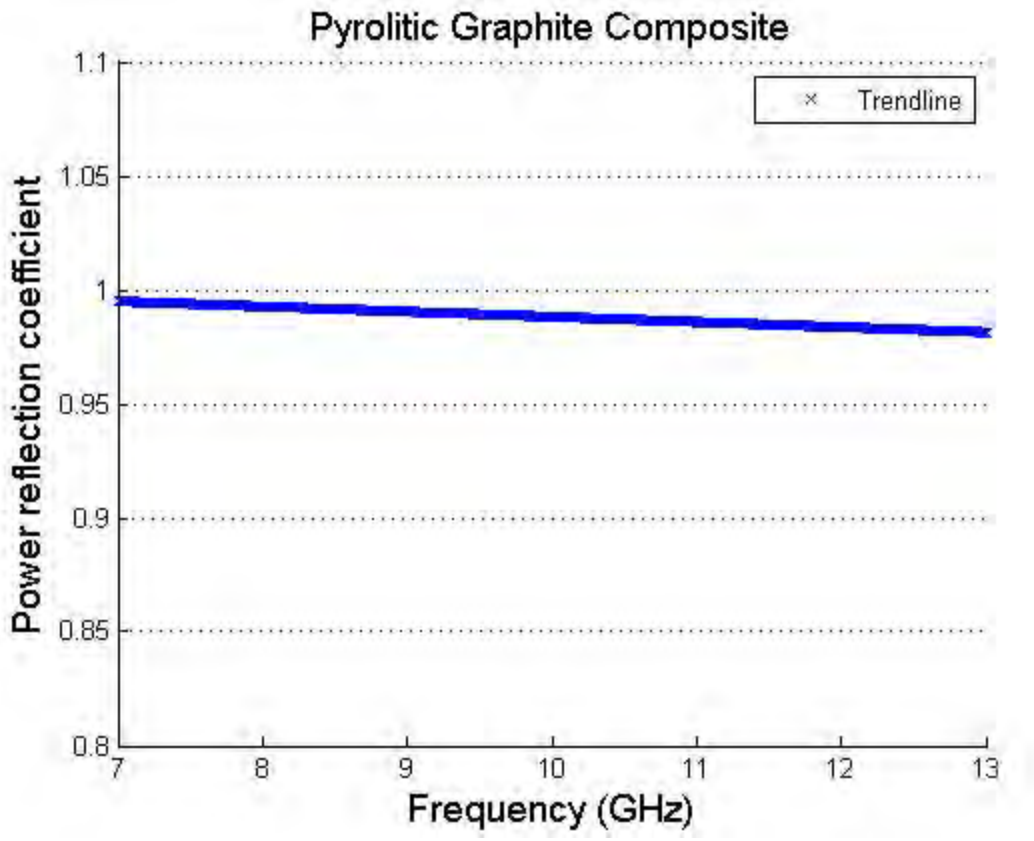

Figure 54: Power coefficient trend line for the pyrolitic graphite composite

4.4 Power coefficient comparison of the materials

For each material, the power coefficients were calculated and presented individually. This section will conduct a comparison of each materials calculated power coefficient trend line to determine the effects there differences have on the power coefficient in the X-band frequency range. Figure 55 and 56 shows the trend lines for the composite materials. Table 3 gives power coefficient values at five distinct frequencies.

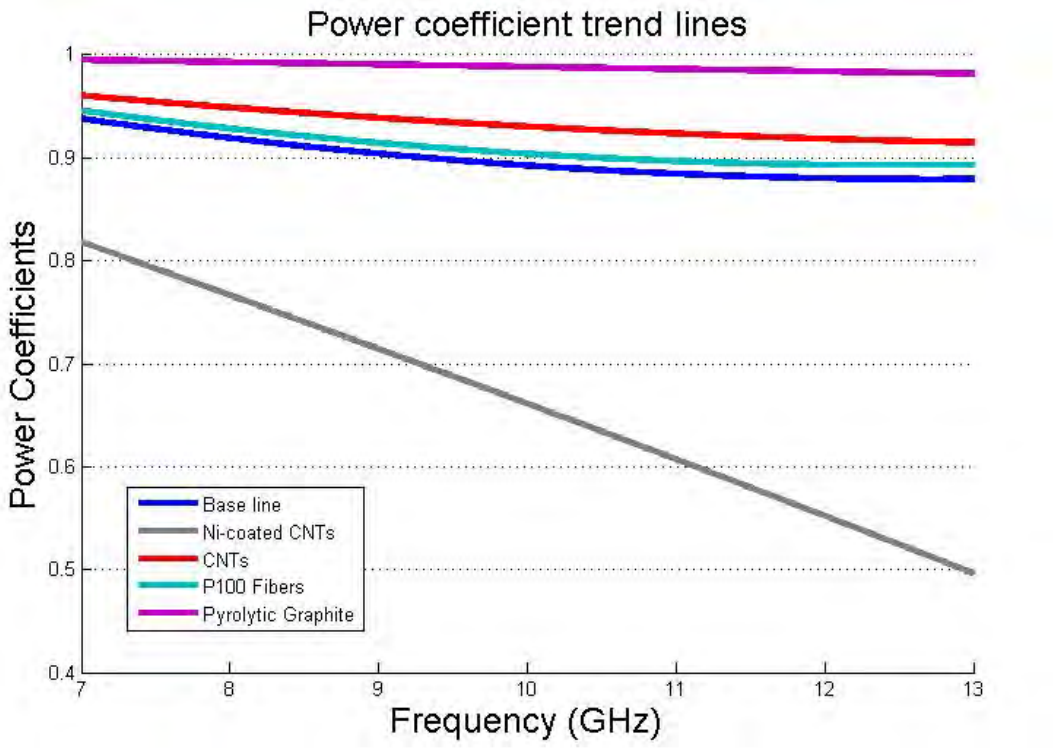

Figure 55: Power coefficient trend lines of the composite materials

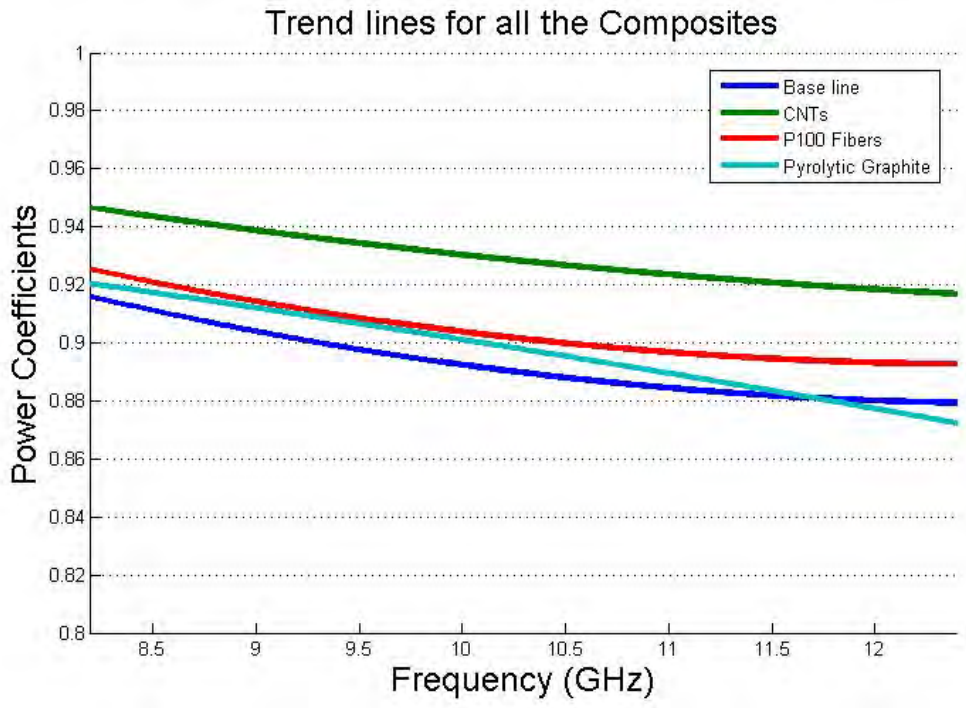

Figure 56: Power coefficient trend lines of the composite materials

Table 3: Frequency versus power coefficients for different materials trend lines

Specific Power Coefficient Data from Trend Lines					
Frequency (GHz)	Baseline	CNTs	Ni-coated CNTs	Pyrolitic Graphite	P100 fibers
8.2	91.6%	94.7%	75.6%	100.8%	92.9%
9	90.4%	93.9%	71.4%	100.8%	91.4%
10	89.2%	93.0%	66.1%	100.7%	90.4%
11	88.5%	92.4%	60.7%	100.6%	89.7%
12.4	87.9%	91.7%	53.0%	100.4%	89.3%
Average	89.5%	93.1%	65.3%	100.6%	90.7%

The addition of CNT, P100 fiber, and pyrolitic graphite to the baseline carbon fiber composite improved the overall power coefficient throughout the X-band frequency range. With the exception of the pyrolitic graphite, the composites power coefficient decreased as the frequency increase. This is expected because as the frequency increase, the wavelengths become smaller and smaller. This increases the ratio between the wavelength and the material's surface roughness. As the roughness of the composite becomes on the order of skin depth, attenuation increases. Skin depth is the distance the EM energy travels into the material, or how deep into the material it penetrates, before the conductivity density is reduced to 1/e of the original value at the material's surface. Skin depth is a function of conductivity, frequency, and a material's permeability. Figure 57 shows how the ratio of surface roughness and skin depth increase the attenuation (or losses). [31]

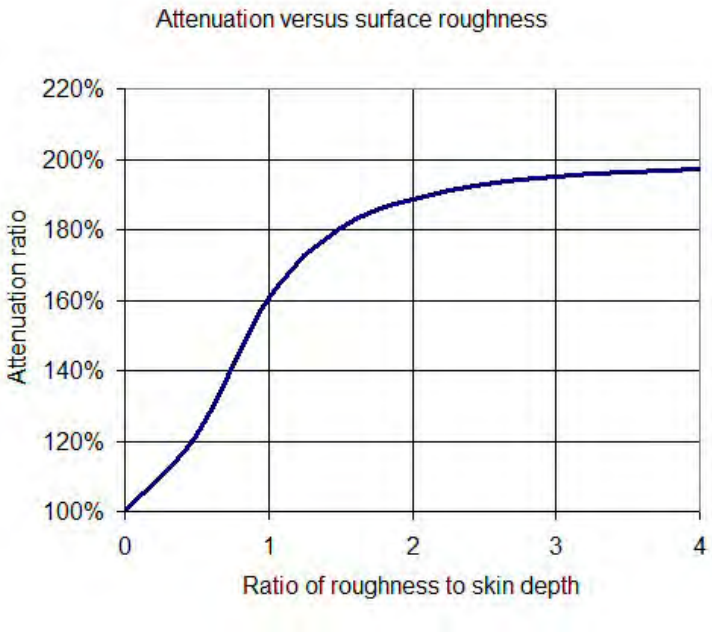

Figure 57: Attenuation versus surface roughness

As the wavelength become smaller, bumps and roughness caused by the fibers weave, resin, and other added materials become relatively larger with respect to the wavelength. For example, the EM wave at 4 GHz with a 15cm wavelength will be less affected by the small surface imperfections of the composites compared to the wavelength of 3cm at 10 GHz.

The addition of the Ni-coated CNTs decreased the power coefficient of the composite across the entire frequency. This is somewhat surprising as Nickel is considered a conductive metal used in a variety of applications. There are two potential reasons why this may occurred. As discussed before, the Ni-coated CNTs may have increased the surface "roughness" due to the additional size of the CNTs from the nickel coating. The CNTs alone were approximately 60nm, but the Ni-coated CNTs received an additional 30nm of the nickel coating. However, at this frequency range the surface

roughness seems unlikely to cause a drop in performance because the wavelengths at this frequency range are larger in comparison to the material's surface roughness.

Another reason the performance may have dropped is due to nickel's large skin depth. As discussed, skin depth is a function of frequency, conductivity, and permeability.

$$\delta_s = \sqrt{\frac{2}{2\pi f \mu \sigma}} \tag{24}$$

Compared to copper, nickel has a much larger skin depth because nickel has larger conductivity and a 200+ times the permeability. However, compared to graphite and carbon, nickel has a much smaller skin depth. Another area of concern is that for a given weight fraction, the Ni-coated CNTs are much heavier than their nickel-less counter parts. Therefore, there are much more of the regular CNTs which create much more interconnects throughout the epoxy resin. This allows electrons to move about more freely.

V. Conclusions and Recommendations

The results were presented after conducting many experiments. Different carbon based composites were manufactured and compared. Not all testing goals were met. The sheet resistivity measurements could not be accomplished. This chapter will draw over all conclusions from the data and have future recommendation for research.

5.1 Conclusions

The objective of this research was to characterize composite materials for use in load bearing waveguides. The waveguide will be designed as a multifunctional part, capable of supporting structural loads and propagating EM energy for use in an antenna array. The study compared the power coefficient of five different composites. Each composite was made of Grafil 34-700 carbon fiber and EPON 862 epoxy. The results show that the baseline composite reflected approximately 89.5% of the RF power. Four different carbon based materials were combined with the carbon fiber epoxy to study their affects on the composite's RF performance: CNTs, nickel coated CNTs, pyrolitic graphite, and P100 fibers.

The CNTs were mixed into the resin and cured in an autoclave with the carbon fiber weave. The study has shown that adding CNTs to a composite improves the composites ability to reflect electromagnetic energy by an average of 3.6%. Additionally, nickel coated CNTs were examined. The results found that the addition of Ni-coated CNTs dramatically reduced the RF performance of the waveguide. The Ni-

coated CNT composite saw a reduction of about 24.2% in the amount of power reflected back.

P100 fibers are aligned and cured onto the baseline composite. The results for the P100 composite show a cyclic pattern in the power coefficient. The P100 composite resulted in a 1.2% increase in performance as compared to the baseline composite, but that value can vary more dramatically depending on where you select the data. Overall it improves the performance over the baseline composite. The pyrolitic graphite composite has the best performance compared to the other tested materials. The addition of the pyrolitic graphite layer resulted in an increase in performance of around 8.4%. The substantial increase is attributed to the atomic structure of the graphite.

The primary goal of this research was to determine the permittivity of the composite materials to calculate the ohmic losses of the tested material in a waveguide design. Unfortunately, the presented NRW algorithm was not able to process the data because there is not enough information to calculate all the unknowns. Still, power reflection coefficients are calculated and offer insight as to how well the material reflects the RF energy.

5.1 Recommendations and Suggestions for Future Work

This research focused on the electrical performance function of the load-bearing waveguide. A parallel study on the effects of the additional carbon based materials to the structural performance of the waveguide would offer valuable information. The information could be used from a systems design level to determine how to tailor the

composite waveguide for this application, and offer inputs to the trade space in designing this multi-functional component. The addition of CNTs improved the electrical performance of the waveguide, but additional research can focus on varying the types, amounts, size, etc of the CNTs to determine if an optimal solution exists to achieve the electrical and mechanical requirements.

Additionally, this research determined the NRW algorithm is not a viable option to determine the permittivity of the composites. To calculate permittivity, a new algorithm must be developed and used. One potential solution is the short circuit line iterative conversion method. [32] This technique is an iterative process that only requires reflection data and a good initial guess to calculate the permittivity.

In addition, an accurate resistivity measurement could not be obtained with the equipment at AFIT. A method needs to be developed to determine the resistivity of the composite materials. With the resistivity and permittivity methods determined, different composites can be compared and the theoretical performance of a waveguide made of these materials can be calculated. From this, a waveguide can be manufactured and tested to verify the model.

Designing a load-bearing composite waveguide offers many challenges and research opportunities across a spectrum of disciplines. There are material, electrical, and mechanical considerations when designing a load-bearing waveguide and research in all these fields is required to formulate an optimal solution. There are many different areas one can explore to help engineer a solution, and it is recommended that the research continue in some form or fashion.

VI. Bibliography

[1] M. Mirotznik, S.Yarlagadda, R. McCauley, and P. Pa, "Broadband Electromagnetic Modeling of Woven Fabric Composites," *IEEE Trans. Microwave Theory and Techniques, vol. 60, no. 1,pp. 158-169*, Jan. 2012.

[2] K. Bal and V. K. Kothari, "Permittivity of woven fabrics: A comparison of dielectric formulas for air-fiber mixture," *IEEE Trans Dielect. Electr. Insulation*, vol. 17, no. 3, pp. 881-889, Jun. 1993

[3] S.C. Nemat-Nasser, A. Amirkhizi, T. Plaisted, J. Isaacs, and S. Nemat-Nasser, "Structural composites with integrated electromagnetic functionality," in *Proc. SPIE*, 2002, vol. 4698, pp. 237-245.

[4] D. Micheli, R.Pastore, C. Apollo, M. Machetti, G. Gradoni, V. Primiani and F. Moglie, "Boradband Electromagnetic Absorbers Using Carbon Nanostructure-based Composites," *IEEE Trans. Microwave Theory and Techniques, vol. 59, no. 10, pp.2633-2646*, Oct. 2012.

[5] Chen, Lin-Feng. Microwave Electronics: Measurement and Materials Characterisation. Weinheim [u.a.: Wiley, 2004. Print.

[6] Balanis, Constantine A. Advanced Engineering Electromagnetics. New York: Wiley, 1989. Print.

[7] Wong, H. -S. Philip, and Deji ,. Akinwande. Carbon Nanotube and Graphene Device Physics. Cambridge [etc.: Cambridge UP, 2011. Print.

[8] Mallick, P. K. Fiber-reinforced Composites: Materials, Manufacturing, and Design. Boca Raton, FL: CRC, 2008. Print.

[9] Sabat, Joseph W. *Structural Response of the Slotted Waveguide Antenna Stiffened Structure Components under Compression*. MS Thesis. Air Force Institute of Technology (AU), Wright-Patterson AFB OH, Mar 2010.

[10] Slepyan, Gregory Ya., Sergey A. Maksimenko, Oleg M. Yevtushenko, and Anton V. Gusakov. "Electronic and Electromagnetic Properties of Nanotubes." Physical Review B 57.16 (1998): 9485-497. Print.

[11] Watts, P. "The Complex Permittivity of Multi-walled Carbon Nanotube–polystyrene Composite Films in X-band." Chemical Physics Letters 378.5-6 (2003): 609-14. Print.

[12] Do, Van Nam, and Thanh Huy Pham. "Graphene and Its One-dimensional Patterns: From Basic Properties towards Applications." Advances in Natural Sciences: Nanoscience and Nanotechnology 1.3 (2010): 033001. Print.

[13] Slepyan, G. Ya., S. A. Maksimenko, O. Yevtushenko, and A. V. Gusakov. "Electrodynamics of Carbon Nanotubes: Dynamic Conductivity, Impedance Boundary Conditions, and Surface Wave Propagation." Physical Review B 60.24 (1999): 17136-7149. Print.

[14] Ra Shuba, M. V., G. Ya. Slepyan, S. A. Maksimenko, C. Thomsen, and A. Lakhtakia. "Theory of Multiwall Carbon Nanotubes as Waveguides and Antennas in the Infrared and the Visible Regimes." Physical Review B 79.15 (2009). Print.

[15] Zhu, Q., L. Wu, S. Sheng, Z. C. Mei, W. F. Liu, W. L. Cai, and L. Z. Yao. "Possibility of Constructing Microwave Antenna with Carbon Nanotubes." Journal of Vacuum Science & Technology B: Microelectronics and Nanometer Structures 25.5 (2007): 1630. Print.

[16] Micheli, D., C. Apollo, R. Pastore, and M. Marchetti. "X-Band Microwave Characterization of Carbon-based Nanocomposite Material, Absorption Capability Comparison and RAS Design Simulation." Composites Science and Technology 70.2 (2010): 400-09. Print.

[17] Highered.mcgraw-hill.com. 5 May 2003. Magraw-HIll Publishing. 16 Feb 2012 <highered.mcgraw-hill.com/sites/dl/free/0072549076/ch07.pdf>

[18] Wagner, R., and Ingvarson, P., 1982. “Synthetic Aperture Radar from CFRP.” In Digest International Geoscience and Remote Sensing Symposium (IGARSS), Vol. 1, Dornier Systems GmBH and Ericsson, IEEE, pp. 4.1-4.6

[19] Institute of Electrical and Electronics Engineers, “The IEEE standard dictionary of electrical and electronics terms”; 6th ed. New York, N.Y., Institute of Electrical and Electronics Engineers, c1997. IEEE Std 100-1996. ISBN 1-55937-833-6 [ed. Standards Coordinating Committee 10, Terms and Definitions; Jane Radatz, (chair)]

[20] www.merriam-webster.com. Encyclopedia Britannica. 16 Feb 2012 <http://www.merriam-webster.com/dictionary/composite>

[21] Rosker, M. Integrated Sensor Is Structure (ISIS). <http://www.darpa.mil/mto/programs/isis/>.

[22] Callus, P. J., 2006. Conformal Load-Bearing Antenna Structure for Australian Defence Force Aircraft. Version 0.1, Australian Defense Science and

Technology Oraganisation, Fishermans Ben, Victoria, Australia.

[23] Mitchell, S."Electromagnetic Wave Propagation: Theory and Application to Bathymetric Lidar Simulation." 19 Dec 2008 <http://ccar.colorado.edu/~semitche/asen6849/EM_propagation.pdf 3>.

[24] IPE Nanotube Primer. 17 Feb 2012. <http://ipn2.epfl.ch/CHBU/NTbasics1.htm>.

[25] M. Y. Han, B. Ozyiluaz, Y. Zhang and P. Kim, Energy band-gap engineering of graphene nanoribbons. *Phys. Rev. Lett.*, 98 (2007) 206805.

[26] X. Li, X. Wang, L. Zhang, S. Lee and H. Dai, Chemically derived, ultrasmooth graphene nanoribbon semiconductors. *Science*, 319 (2008) 1229-32

[27] " Momentive.com - EPON Resin 862." *Momentive.com - World Leader in Specialty Chemicals and Materials*. N.p., n.d. Web. 27 Feb. 2012. <http://www.hexion.com/Products/TechnicalDataSheet.aspx?id=3950>.

[28] Zhu, J., Peng, H., Rodriguez-Macias, F., Margrave, J., Khabashesku, V., Imam, A., Lozano, K., Barrera, E. *Reinforcing epoxy polymer composites through covalent integration of functionalized nanotubes.* Advanced Functional Materials, 2004. **14**(7): p. 643-648.

[29] Theodore, Martin , Mahesh Hosur, Johnathan Thomas, and Shaik Jeelani. "ICCM - Home Page." *ICCM - Home Page*. International Committee on Composite Materials , n.d. Web. 23 Feb. 2012. <http://www.iccm-central.org/Proceedings/ICCM16proceedings/contents/pdf/MonA/MoAA2-01sp_theodorem222779p.pdf>.

[30] Eletskii, A. "Transport propeties of carbon nanotubes." *Physics-Uspekhi* 52 (2009): 209-224. Print.

[31] Edwards, Terry, and a Wiley book.. "Surface Roughness - Microwave Encyclopedia - Microwaves101.com." *Microwaves101.com - A practical resource covering the fundamental principles of microwave design*. N.p., n.d. Web. 27 Feb. 2012. <http://www.microwaves101.com/encyclopedia

[32] "Measurement of dielectric material properties." *http://www.rohde-schwarz.cz/*. Version RAC0607-0019. Rhode and Schwarz, n.d. Web. 25 Feb. 2012. <www.rohde-schwarz.cz/file_3463/RAC-0607-0019.pdf>.

REPORT DOCUMENTATION PAGE		*Form Approved* *OMB No. 0704–0188*
The public reporting burden for this collection of information is estimated to average 1 hour per response, including the time for reviewing instructions, searching existing data sources, gathering and maintaining the data needed, and completing and reviewing the collection of information. Send comments regarding this burden estimate or any other aspect of this collection of information, including suggestions for reducing this burden to Department of Defense, Washington Headquarters Services, Directorate for Information Operations and Reports (0704–0188), 1215 Jefferson Davis Highway, Suite 1204, Arlington, VA 22202–4302. Respondents should be aware that notwithstanding any other provision of law, no person shall be subject to any penalty for failing to comply with a collection of information if it does not display a currently valid OMB control number. PLEASE DO NOT RETURN YOUR FORM TO THE ABOVE ADDRESS.		
1. REPORT DATE (DD–MM–YYYY) 29-02-2012	2. REPORT TYPE Master's Thesis	3. DATES COVERED *(From — To)* 7 April 10 – 22 March 2012
4. TITLE AND SUBTITLE Material Characterization for Composite Materials in Load Bearing Wave Guides		5a. CONTRACT NUMBER 5b. GRANT NUMBER 5c. PROGRAM ELEMENT NUMBER
6. AUTHOR(S) Almodovar, Gabriel, Capt, USAF		5d. PROJECT NUMBER 5e. TASK NUMBER 5f. WORK UNIT NUMBER
7. PERFORMING ORGANIZATION NAME(S) AND ADDRESS(ES) Air Force Institute of Technology Graduate School of Engineering and Management (AFIT/ENY) 2950 Hobson Way WPAFB OH 45433-7765		8. PERFORMING ORGANIZATION REPORT NUMBER AFIT/GAE/ENY/12-M01
9. SPONSORING / MONITORING AGENCY NAME(S) AND ADDRESS(ES) Mr William Baron (937) 798-4946 William.Baron@wpafb.af.mil AFRL/RB 2130 8TH ST B20045 R121 WPAFB, OH 45433		10. SPONSOR/MONITOR'S ACRONYM(S) AFRL/RB 11. SPONSOR/MONITOR'S REPORT NUMBER(S)
12. DISTRIBUTION / AVAILABILITY STATEMENT APPROVED FOR PUBLIC RELEASE; DISTRIBUTION UNLIMITED		
13. SUPPLEMENTARY NOTES This material is declared a work of the U.S. Government and is not subject to copyright protection in the United States.		
14. ABSTRACT This study will establish a methodology to examine samples of composite material for application in a load bearing waveguide. The composite material will operate in a specific frequency range for applications in small RPAs. A graphite epoxy stiffening component will be primarily considered. Different nickel, graphene, and carbon nanotube (CNT) coatings and films will be applied to the graphite epoxy. Tests will determine the material's radio frequency (RF) performance for application as an antenna/waveguide component. The study will use scattering (S) parameters determined from a network analyzer to collect these data. The S parameters will then be used to resolve the composites permittivity and reflectivity and allow an estimation of a full scale waveguides performance made from pretested composite material.		
15. SUBJECT TERMS Waveguide, Composite, X-band, Carbon nanotubes, grapheme, permittivity		

16. SECURITY CLASSIFICATION OF:			17. LIMITATION OF ABSTRACT	18. NUMBER OF PAGES	19a. NAME OF RESPONSIBLE PERSON Dr. Anthony Palazotto, AFIT/ENY
a. REPORT U	b. ABSTRACT U	c. THIS PAGE U	UU	100	19b. TELEPHONE NUMBER (Include Area Code) (937) 785-3636 x4599